Εφαρμοσμένη & Περιβαλλοντική Γεωχημεία

2023-24

Διδάσκων

Δρ. Χαρίλαος Τσίκος

Επίκουρος Καθηγητής

htsikos@upatras.gr

CIA: $[Al_2O_3/(Al_2O_3+Na_2O+K_2O+CaO)]*100$

CIA: Δείκτης χημικής εξαλλοίωσης (Chemical Index of Alteration)

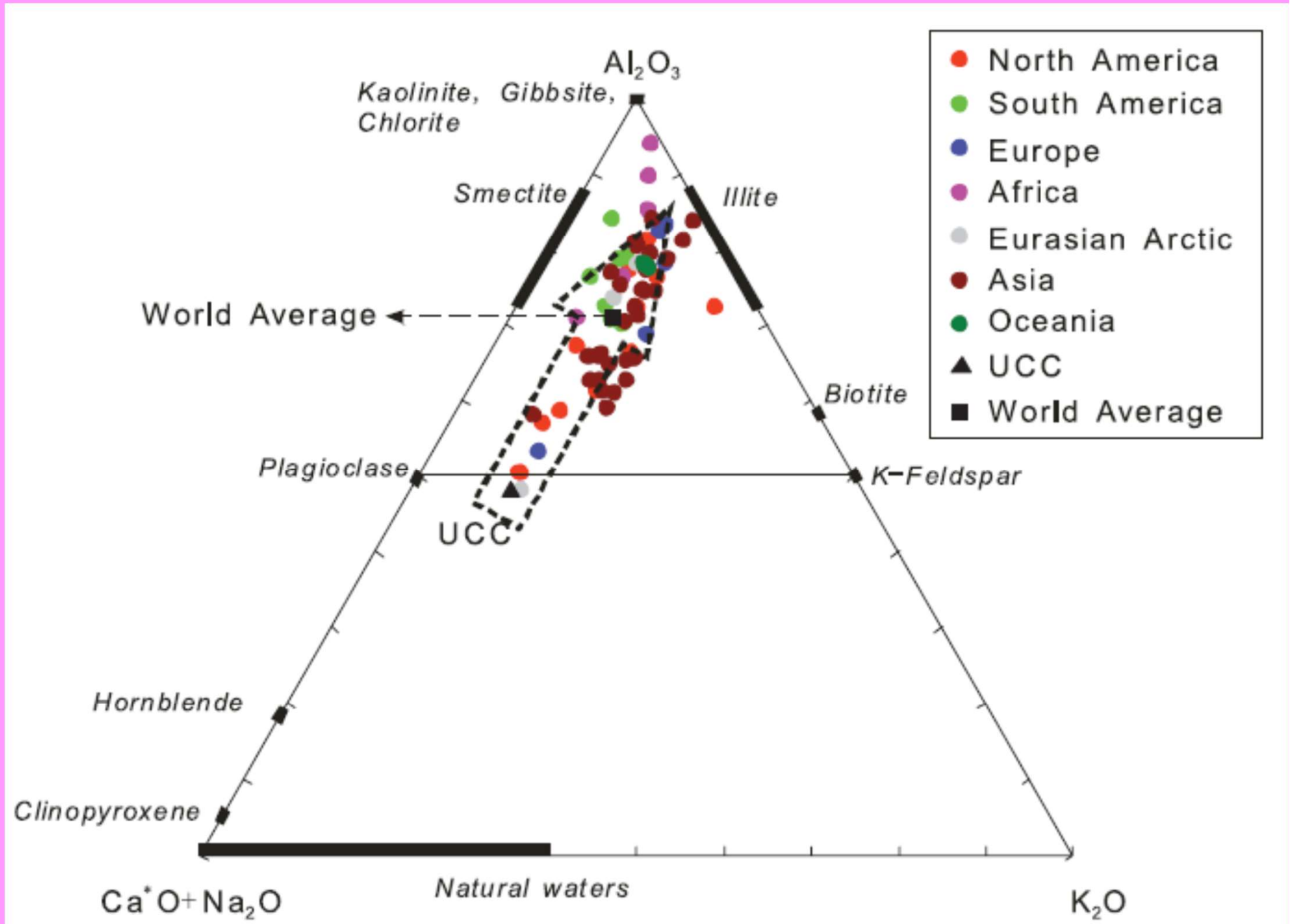

Εφαρμοσμένη & Περιβαλλοντική Γεωχημεία 2023-24

Μεταλλογένεση μεικτών θειούχων στο θαλάσσιο περιβάλλον

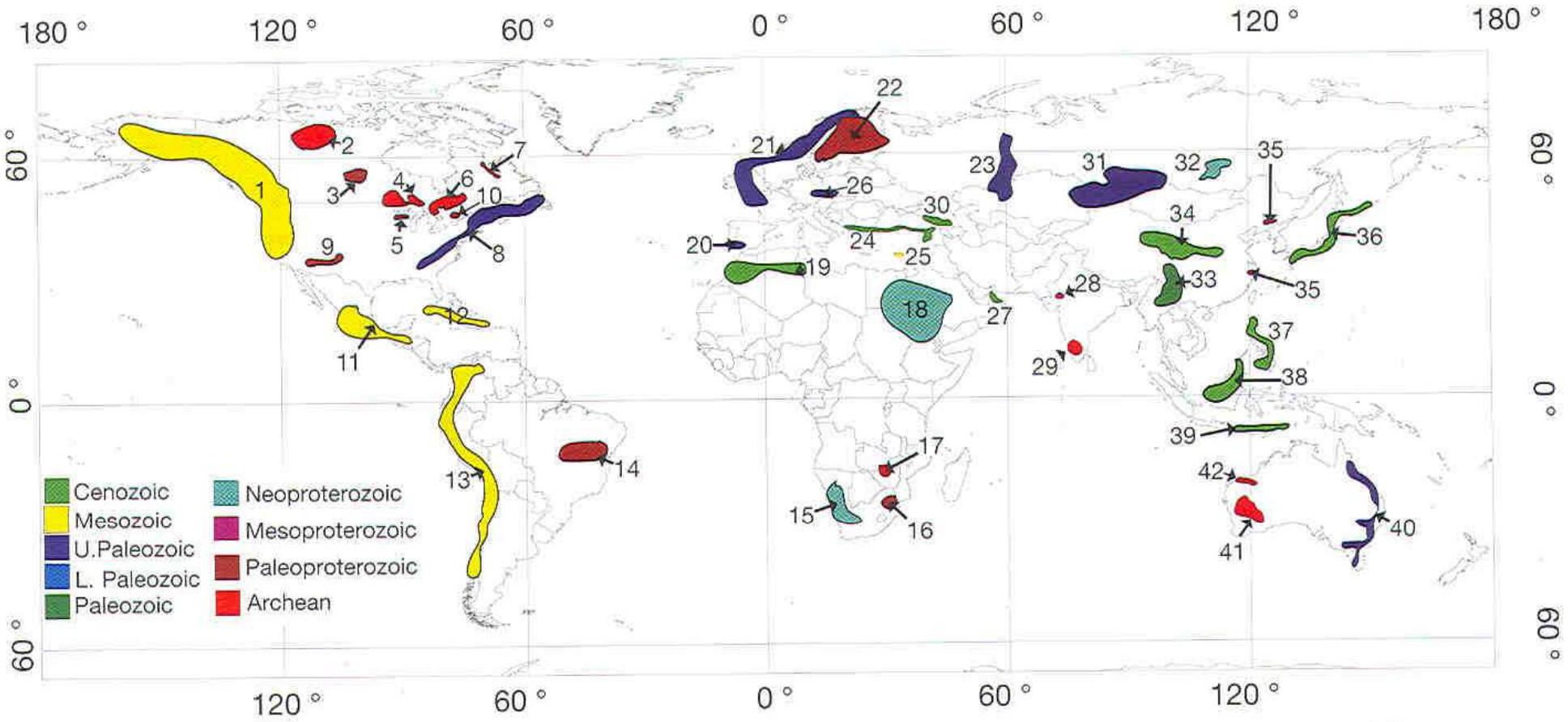

Location of principal orogens containing VMS deposits, classified by Era. See Appendix Table A1 for list of deposits and ages. 1 = northern Cordilleran, 2 = Slave (Kenoran), 3 = western Trans Hudson, 4 = western Superior (Kenoran), 5 = Penokean (Trans Hudson), 6 = Superior (Kenoran), 7 = Labrador trough (Trans Hudson), 8 = Appalachian, 9 = Yavapai, 10 = Sudbury impact, 11 = central Cordillera, 12 = Caribbean arcs, 13 = southern Cordillera, 14 = Amazonian, 15 – Gariep-Damara, 16 = Magondi, 17 = Barberton, 18 = Pan African (Arabian), 19 = Atlas (Alpine), 20 = Iberian (Hercynian), 21 = Caledonides, 22 = Svecokarelian, 23 = Uralian (Caledonian; Hercynian), 24 = Pontides (Tethyan), 25 = Troodos (Tethyan), 26 = Bohemian (Variscan), 27 = Semail (Tethyan), 28 = Aravalli, 29 = Dharwar, 30 = Caucasian, 31 = Altaides (Hercynian), 32 = Baika-Vitim (Caledonian), 33 = north Qilian (Caledonian), 34 = Indonesian platform (Tethyan), 35 = Sino-Korean (Tethyan), 36 = Japan-Kurile Arcs (Tethyan), 37 = Philippines arc (Tethyan), 38 = Kalimantan arc (Tethyan), 39 = Banda arc (Tethyan), 40 = Tasman, 41 = Yilgarn, 42 = Pilbara.

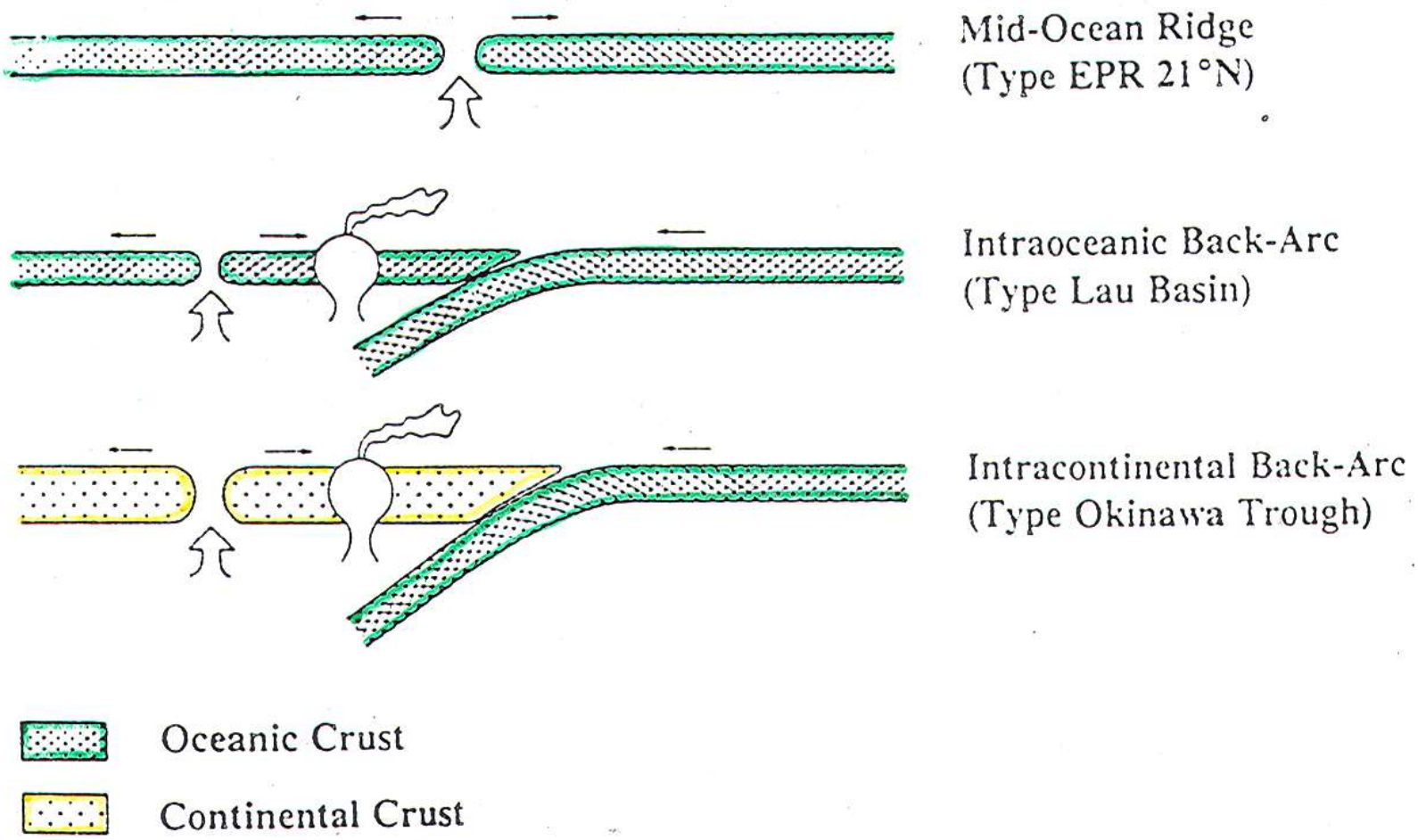

Different environments of seafloor spreading associated with hydrothermal systems and polymetallic massive sulfide deposits.

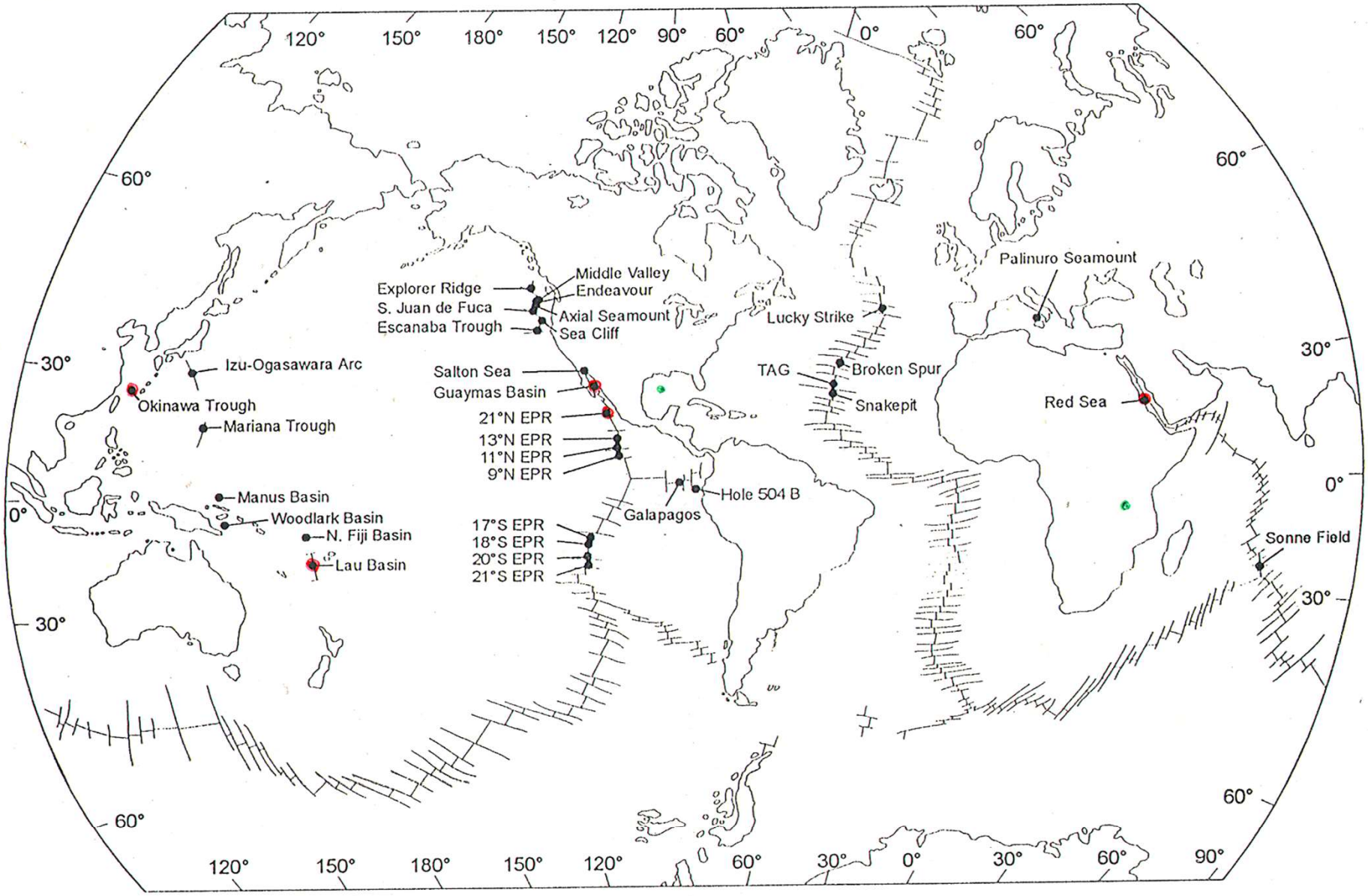

Location of hydrothermal systems and polymetallic massive sulfide deposits at the modern seafloor.

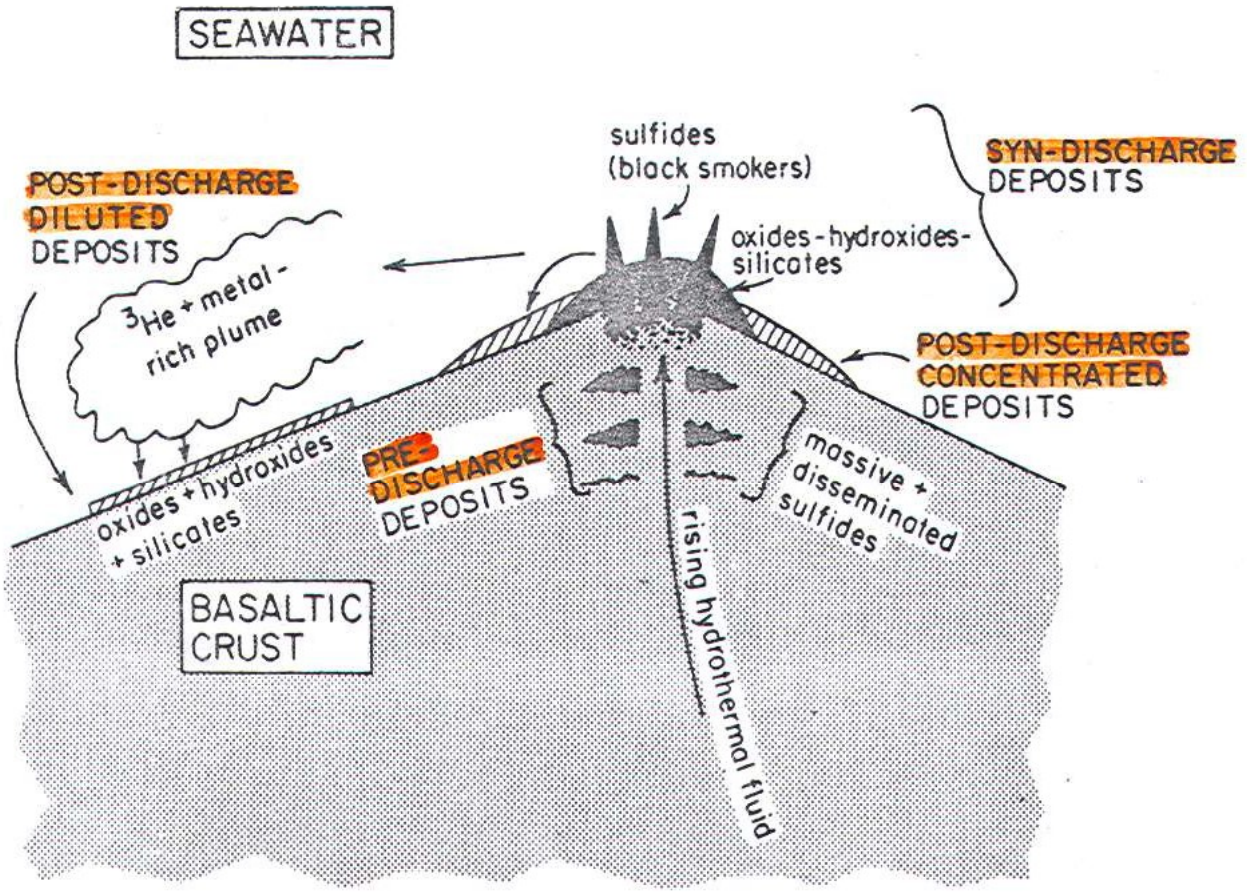

Schematic representation of different types of metal deposits resulting from sub-sea floor hydrothermal circulation in the axial zone of accretion. Intra-sedimentary deposits are not represented.

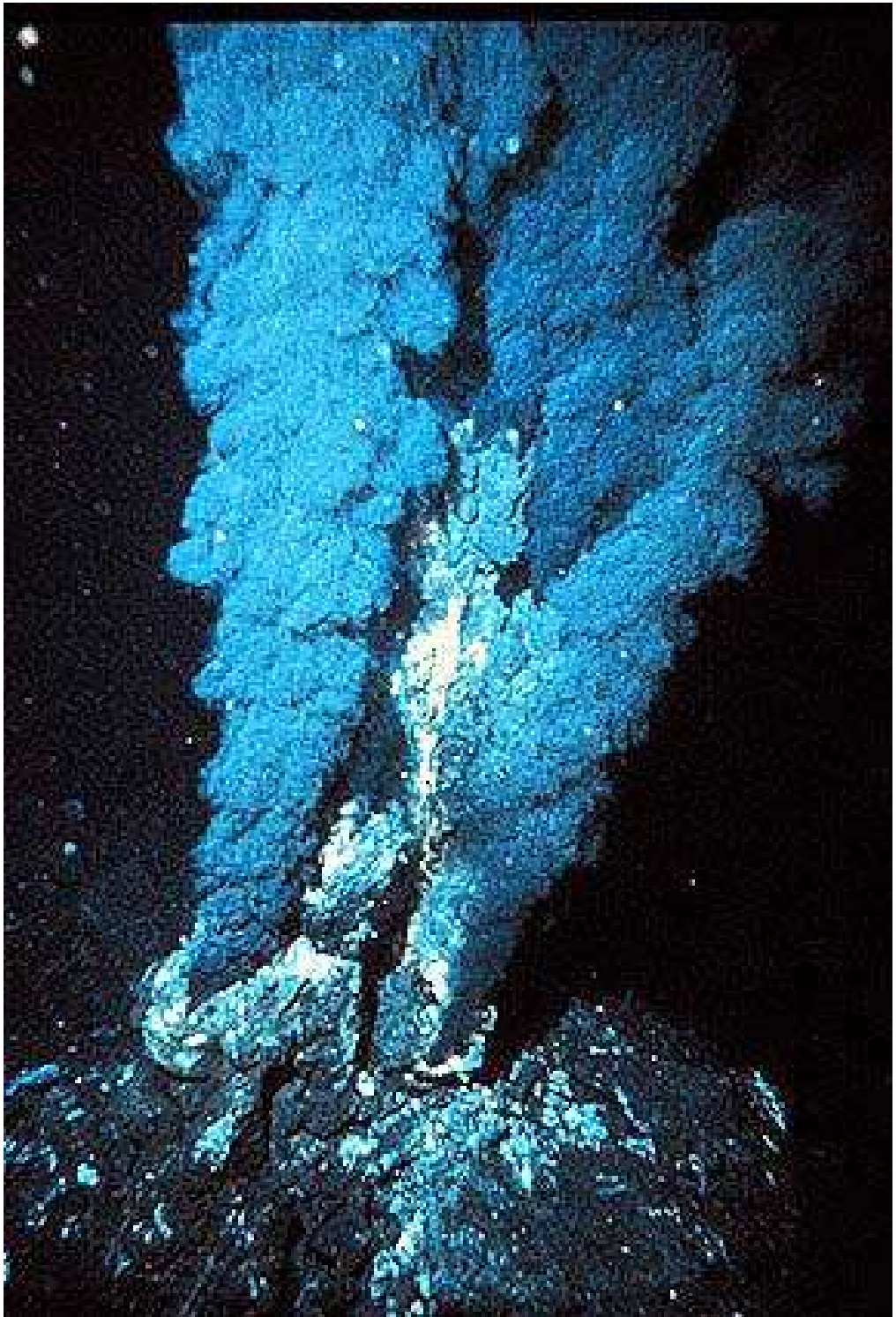

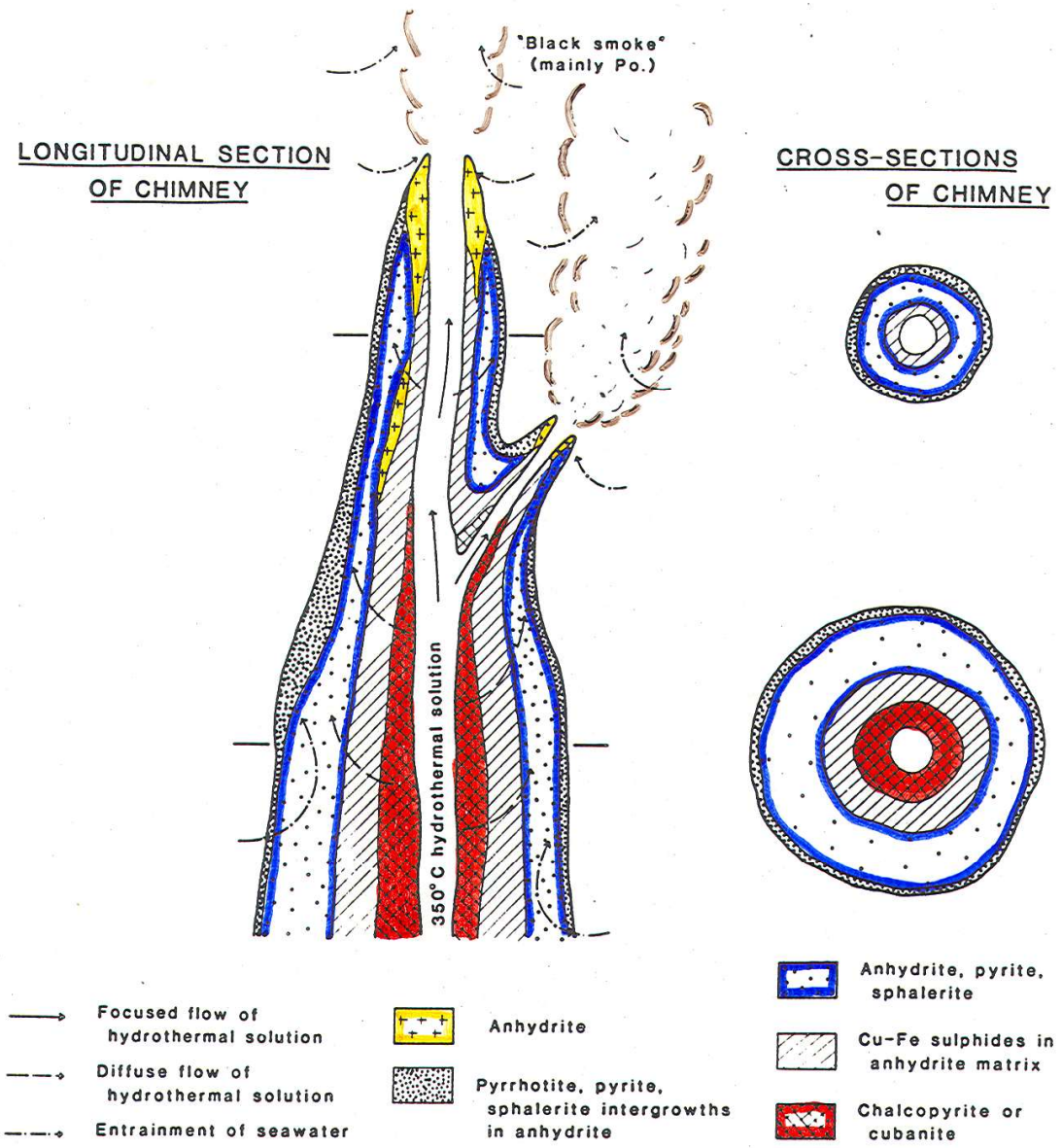

Characteristics of mineral zonation of a modern "black smoker" sulphide chimney. (After Haymon and Kastner, 1981; Haymon, 1983).

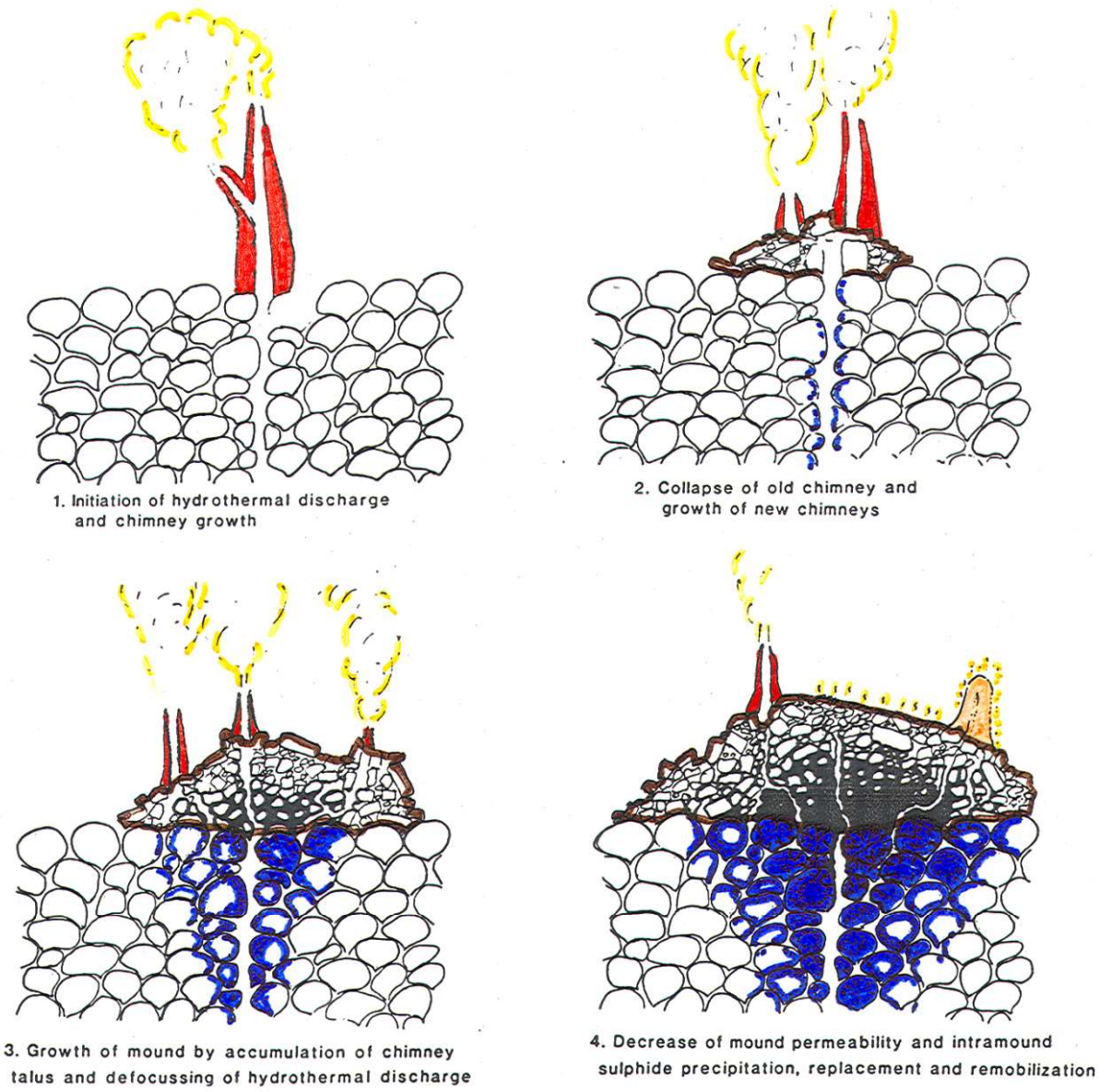

Schematic representation of the growth of a modern mound-chimney sulphide deposit. (Based on the descriptions by Hekinian and Foquet, 1985; Goldfarb et al., *1983; Jonasson* et al., *1986).*

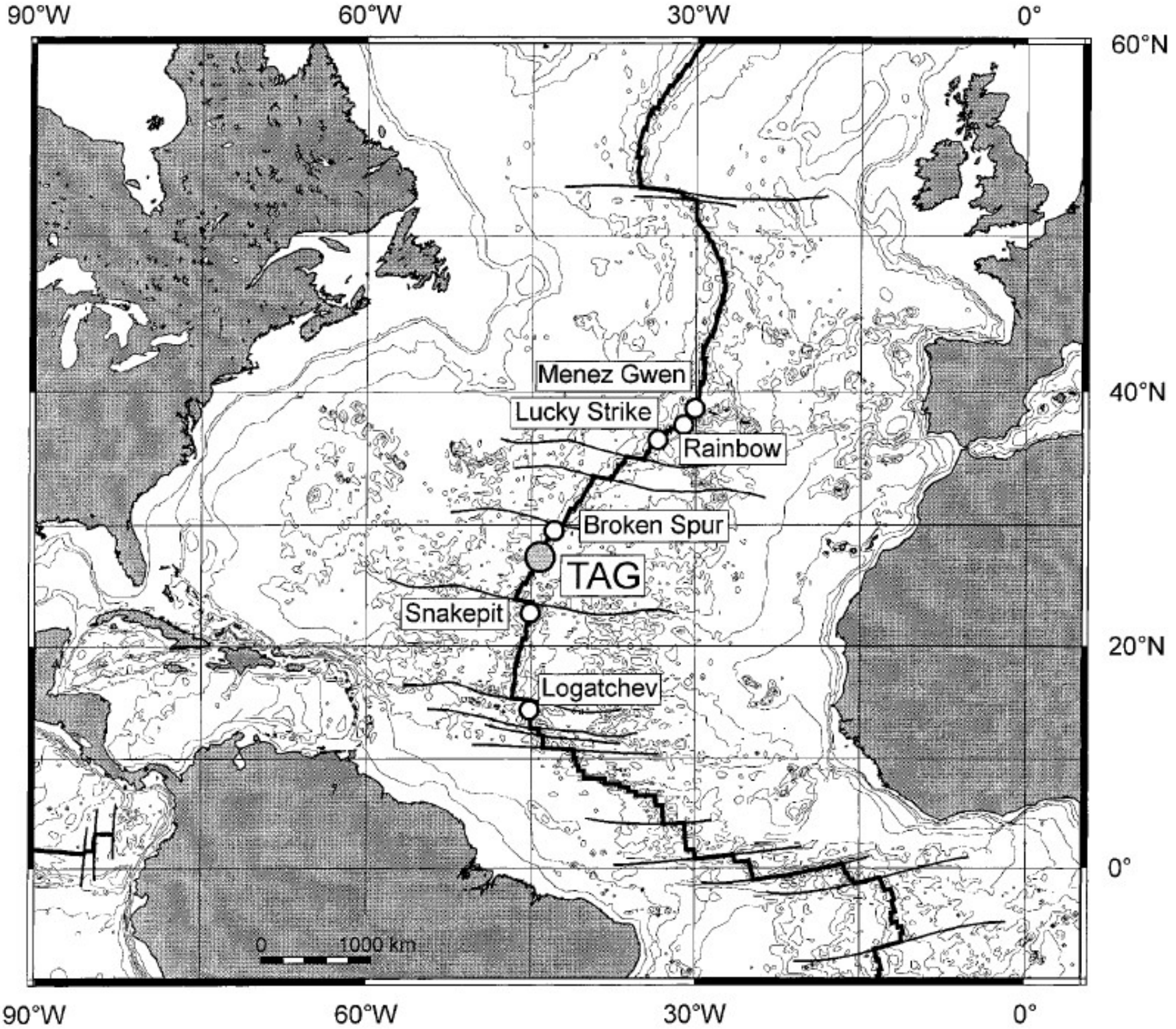
90°W
60°W
30°W
0°
60°N
40°N
20°N
0°
Menez Gwen
Lucky Strike
Rainbow
Broken Spur
TAG
Snakepit
Logatchev
0
1000 km

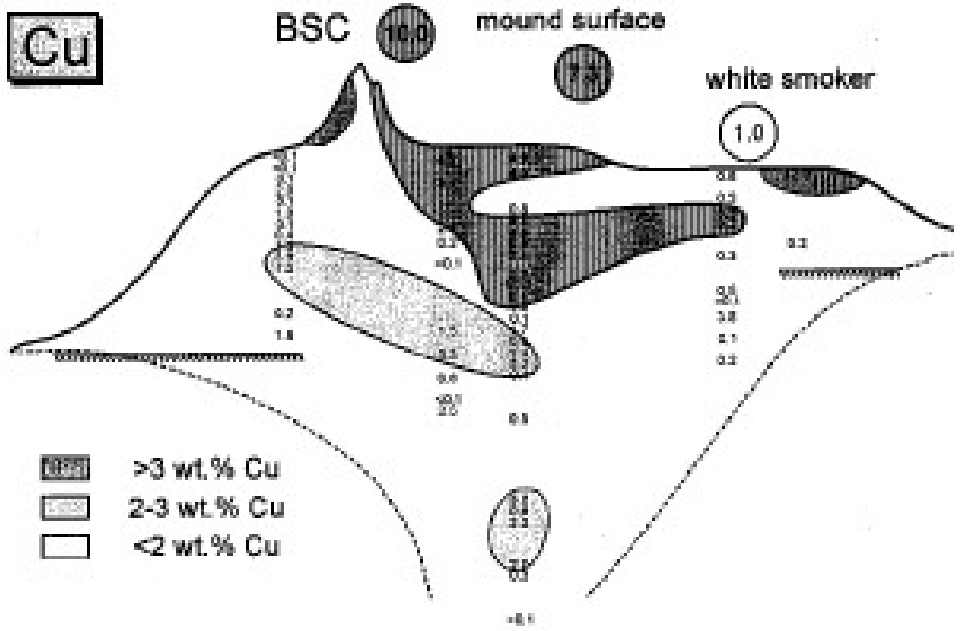
Cu
BSC
mound surface
white smoker
>3 wt.% Cu
2-3 wt.% Cu
<2 wt.% Cu

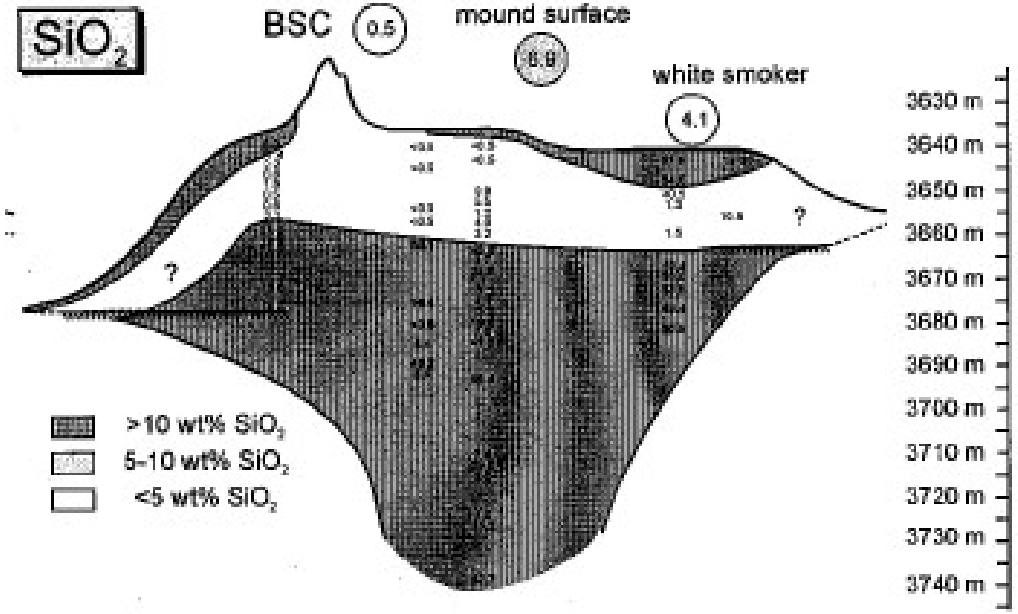
SiO2
BSC
mound surface
white smoker
>10 wt% SiO2
5-10 wt% SiO2
<5 wt% SiO2
3630 m
3640 m
3650 m
3660 m
3670 m
3680 m
3690 m
3700 m
3710 m
3720 m
3730 m
3740 m

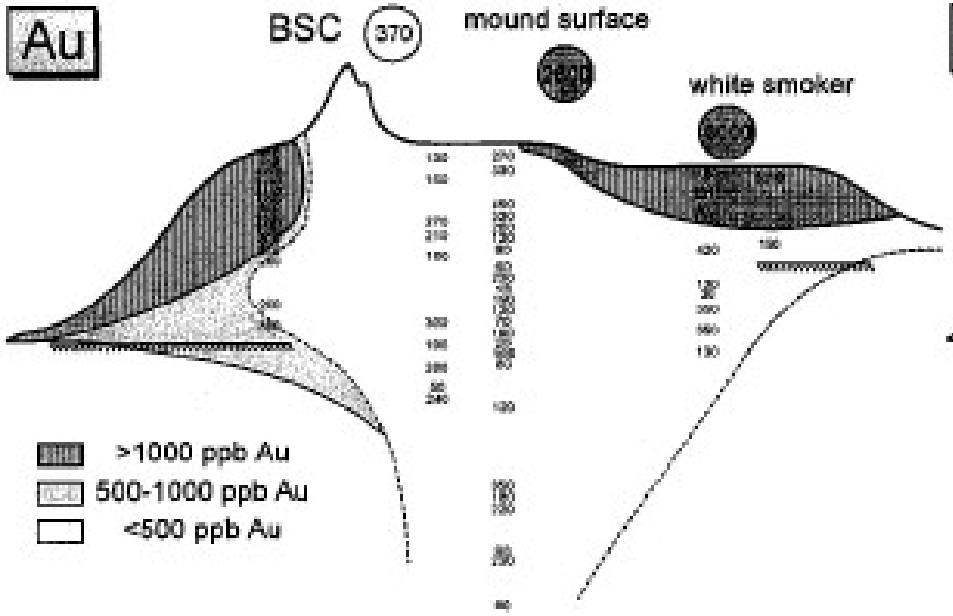
Au
BSC
mound surface
white smoker
>1000 ppb Au
500-1000 ppb Au
<500 ppb Au

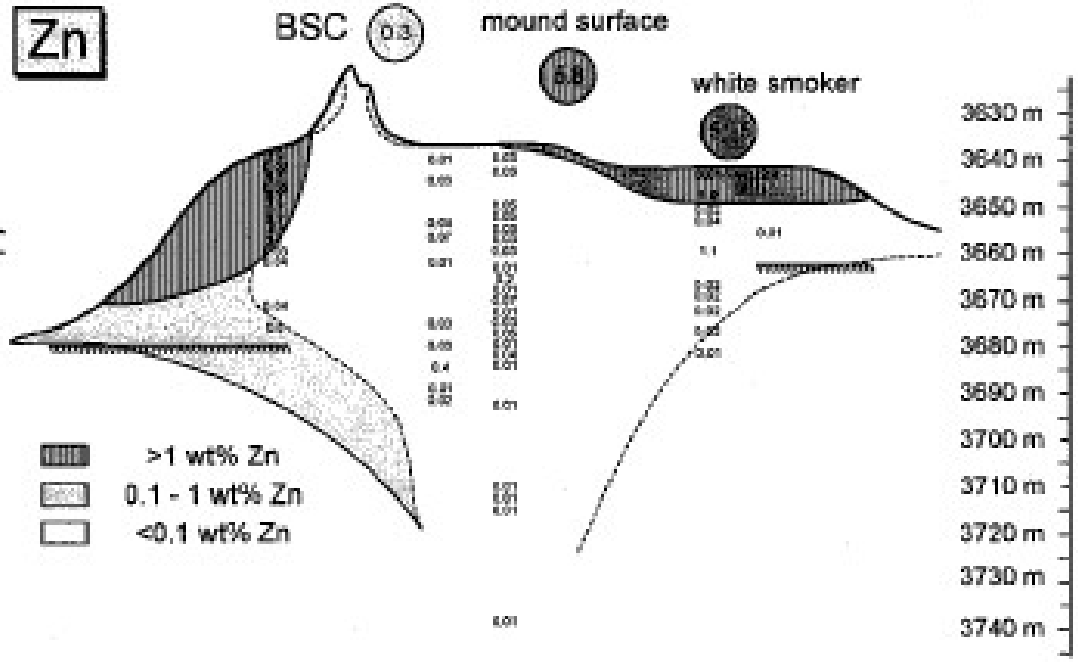
Zn
BSC
mound surface
white smoker
>1 wt% Zn
0.1 - 1 wt% Zn
<0.1 wt% Zn
3630 m
3640 m
3650 m
3660 m
3670 m
3680 m
3690 m
3700 m
3710 m
3720 m
3730 m
3740 m

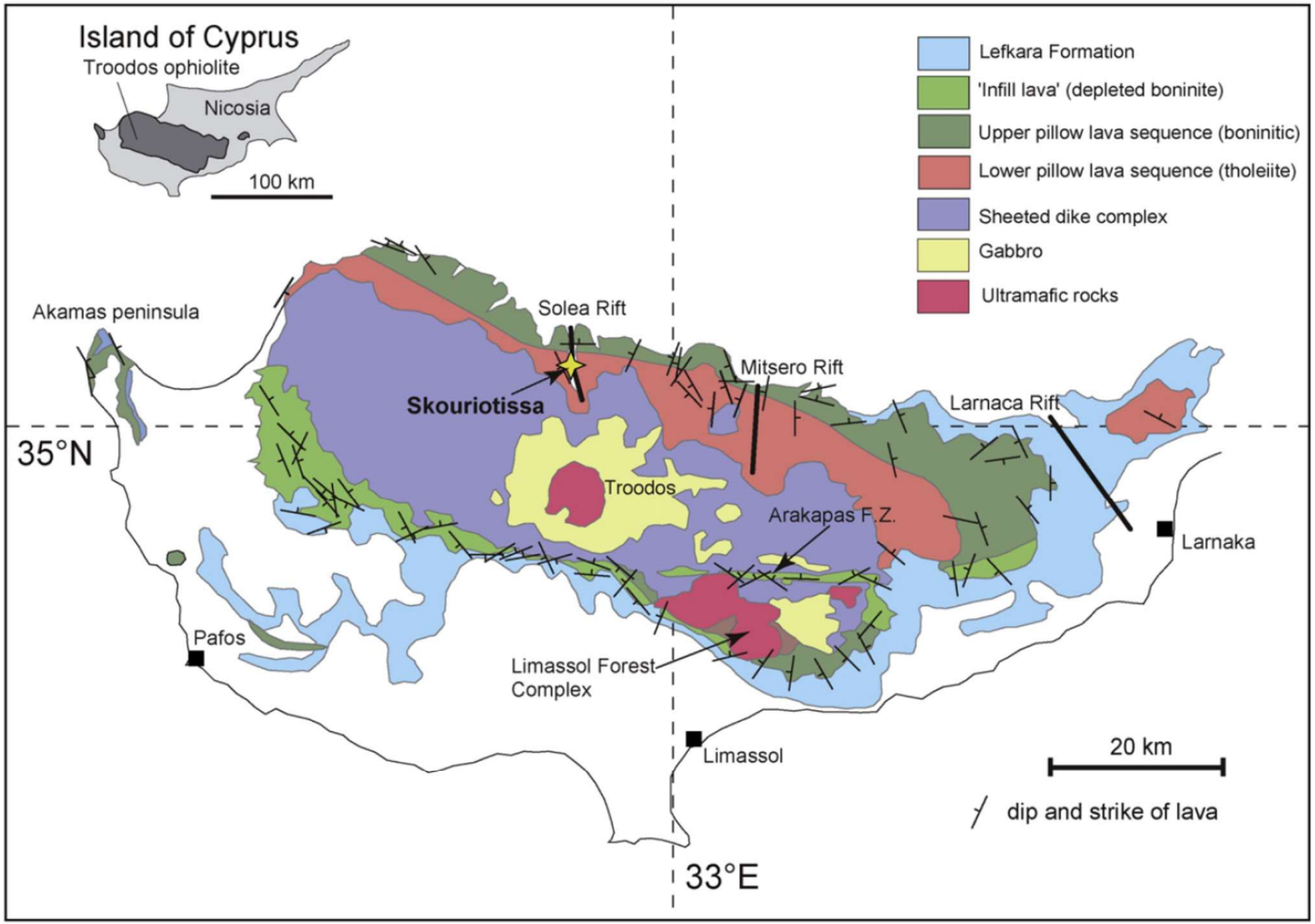

Simplified map of the Troodos ophiolite, modified after Osozawa et al. (2012). The magmatic rocks are of Late Cretaceous age (90–92 Ma, Turonian; Mukasa and Ludden, 1987), while the carbonate sedimentation represented by the Lefkara formation started during Maastrichtian time (66–72 Ma; Robertson, 1977). Abbreviations: F. Z.=fracture zone.

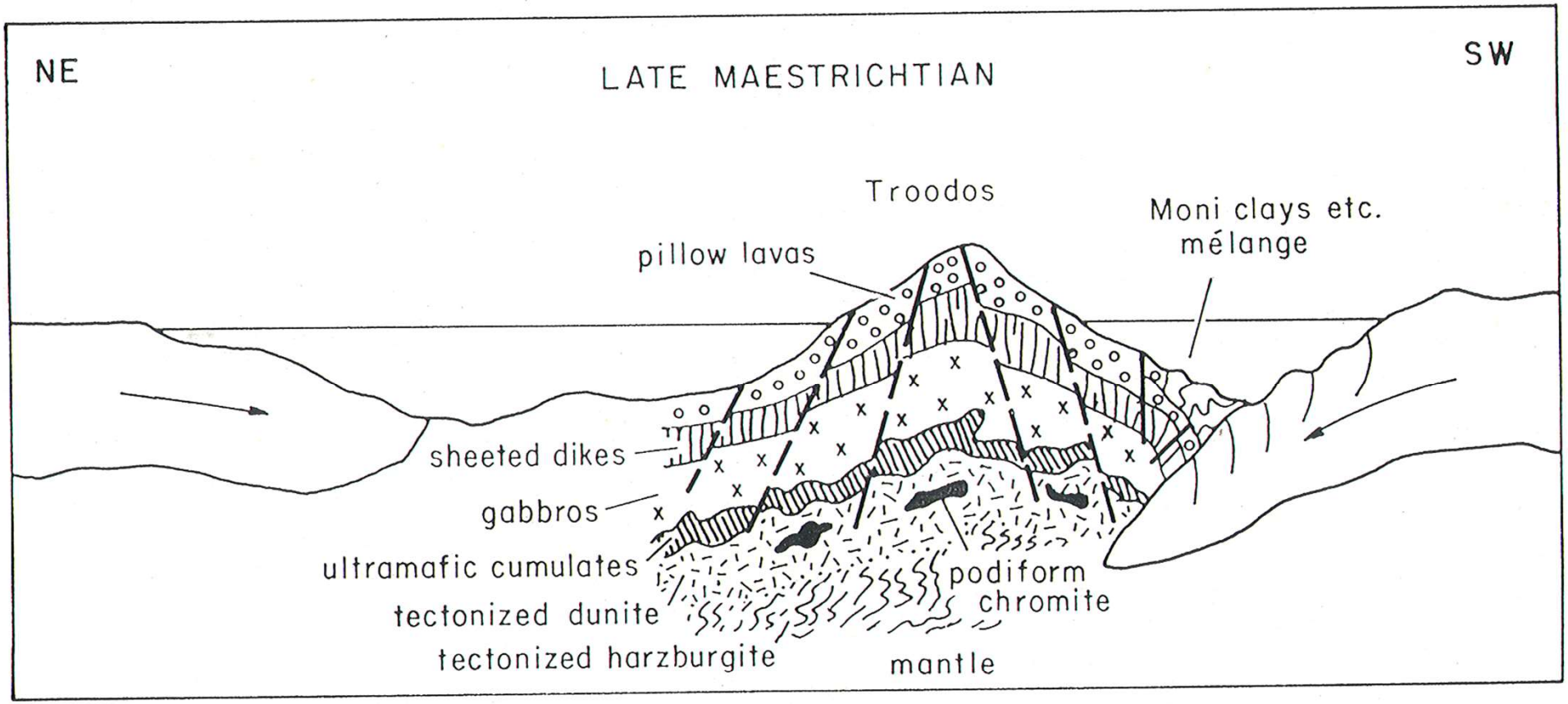

. Schematic cross-section to explain uplift of the Troodos ophiolite complex to its present position (from Searle and Panayiotou 1980)

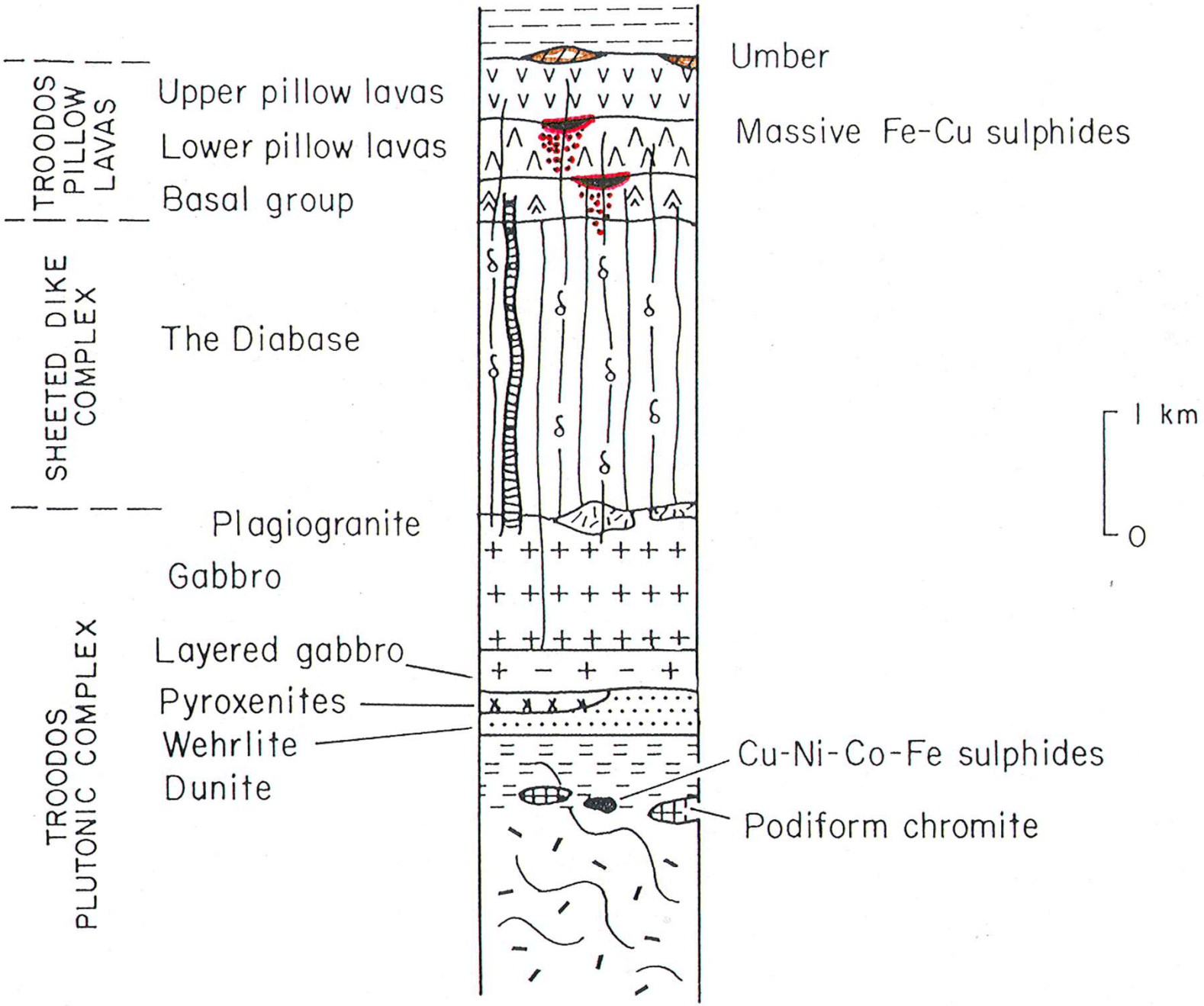

Lithostratigraphic section of the Troodos Ophiolite (from Searle and Panayiotou 1980)

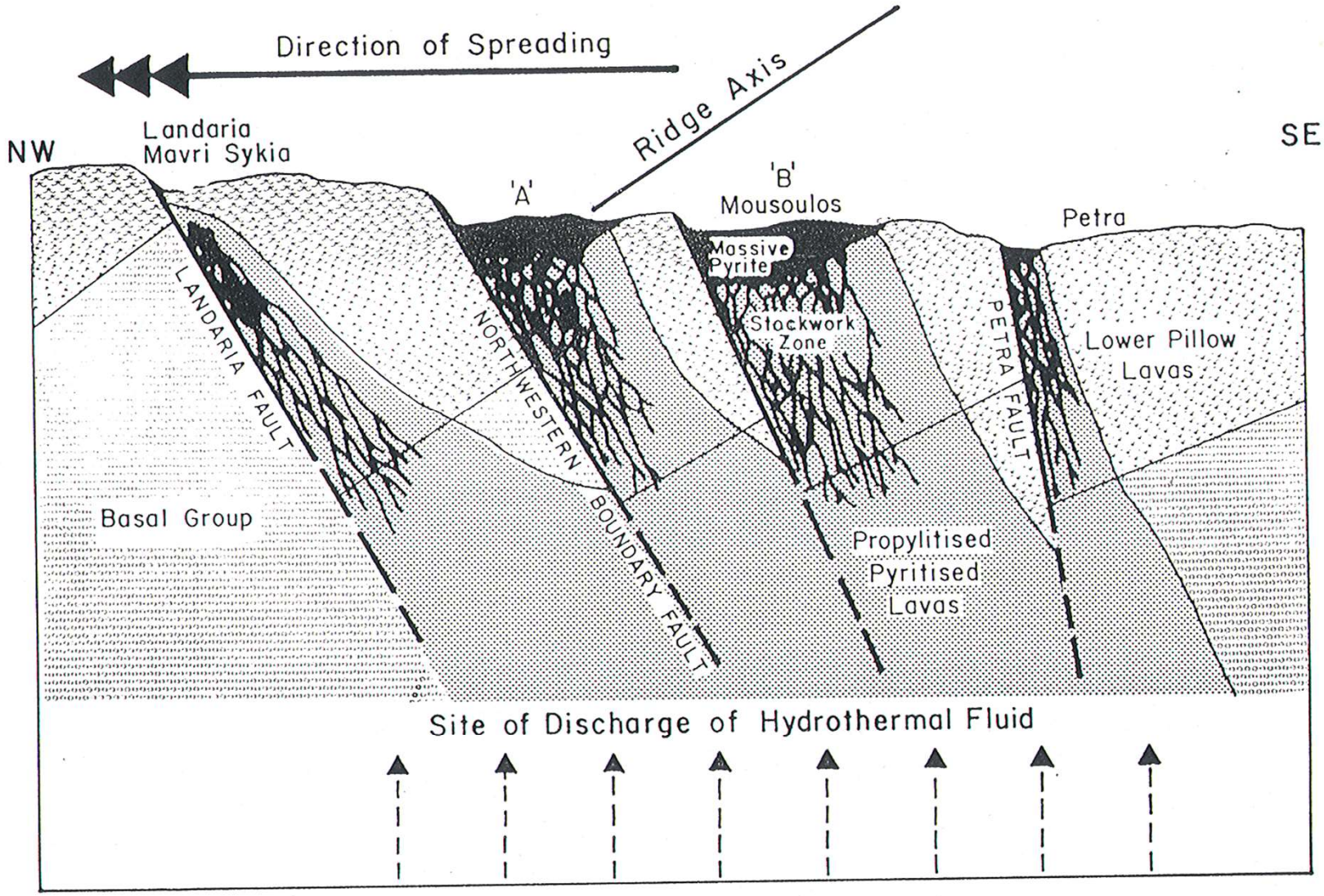

Diagrammatic illustration of the environment of formation of the Kalavasos ore deposits (from Adamides 1980)

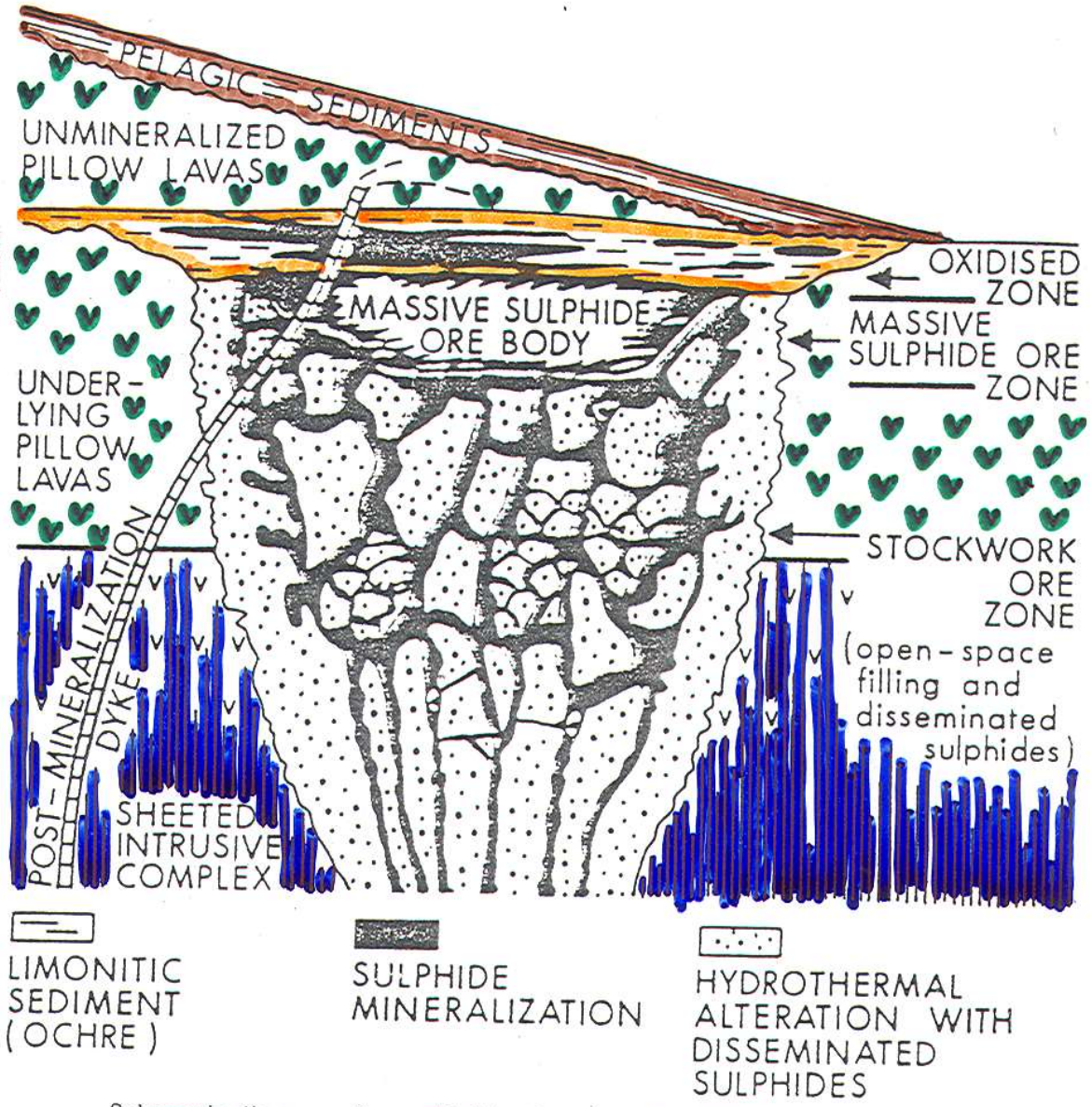

Schematic diagram of an ophiolitic (Cyprus-type) volcanogenic sulphide ore deposit (modified after Hutchinson and Searle, 1971).

The section shows the surficially oxidized massive pyritic lens, which is intercalated within the metabasic pillow lavas, the underlying pipe-shaped stockwork of hydrothermally metamorphosed and mineralized material which extends down into the dyke complex, and the fact that the sulphide ore bodies are usually overlain by unmineralized basaltic pillow lavas, which are in turn overlain by pelagic marine sediments.

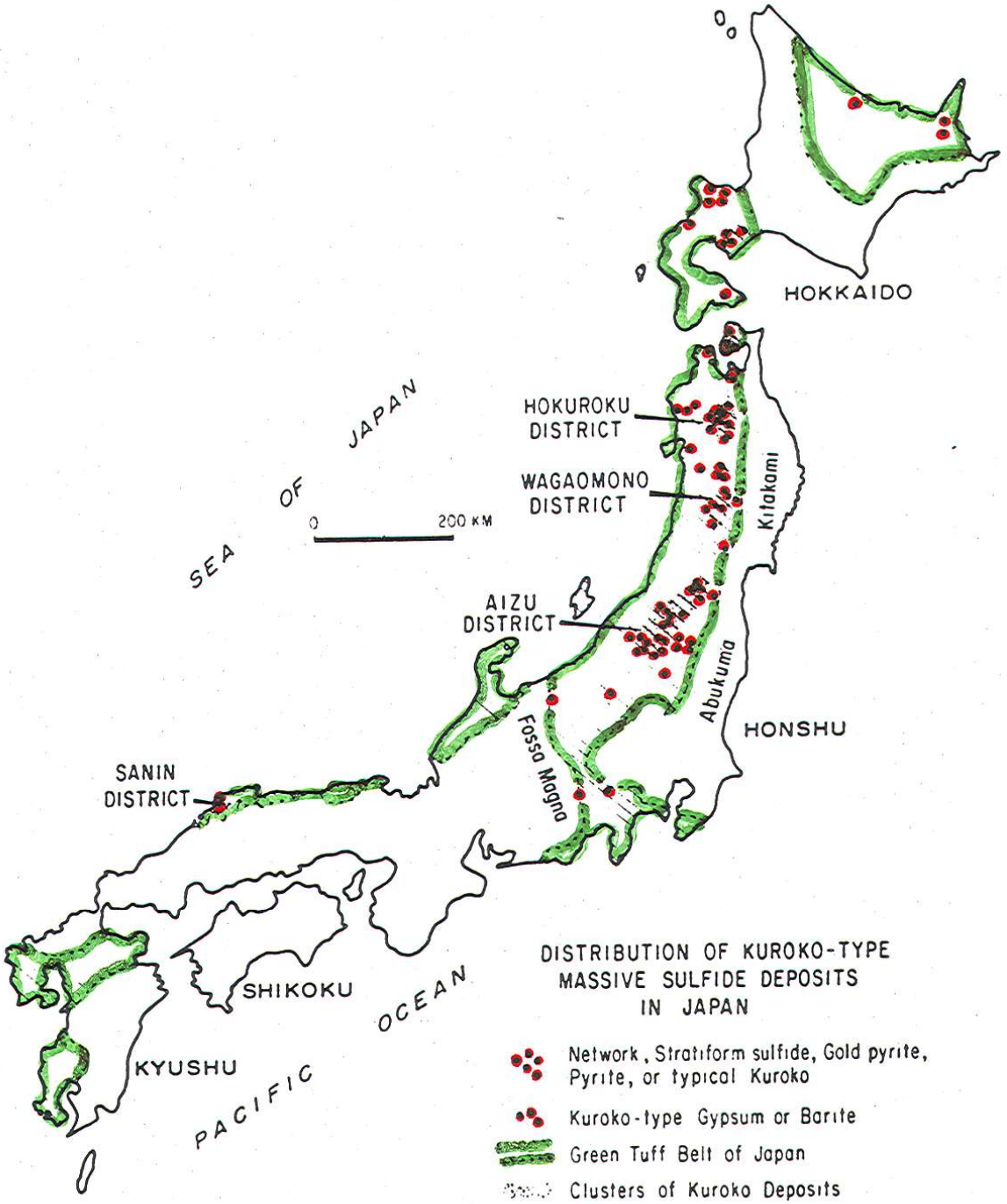

The distribution of the Green Tuff belt of Japan and the Kuroko-type massive sulfide deposits within it. Major mining districts are labeled and ore deposit clusters outlined. Simplified slightly from Sato (1974, fig. 2).

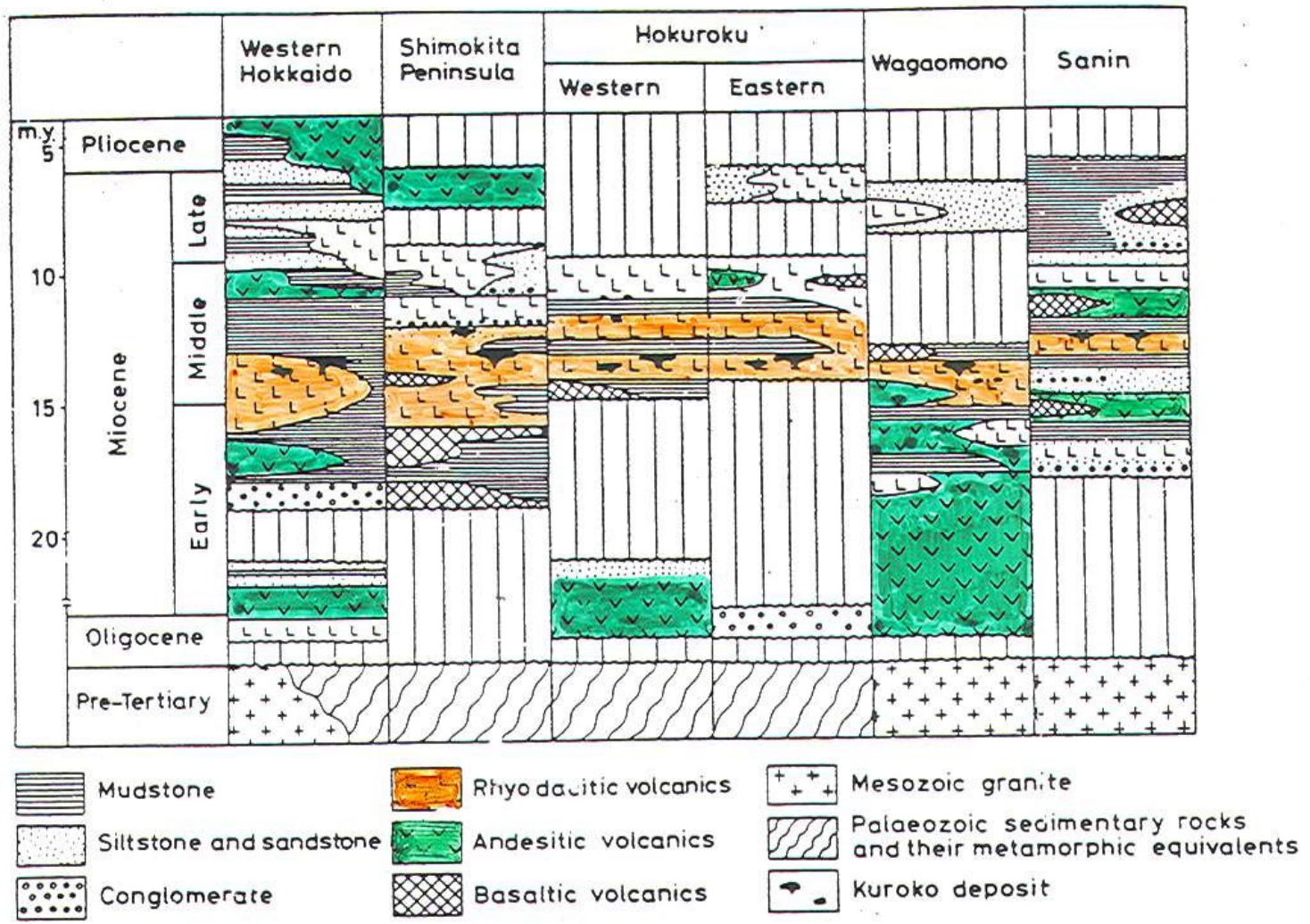

Stratigraphic positions of Kuroko deposits

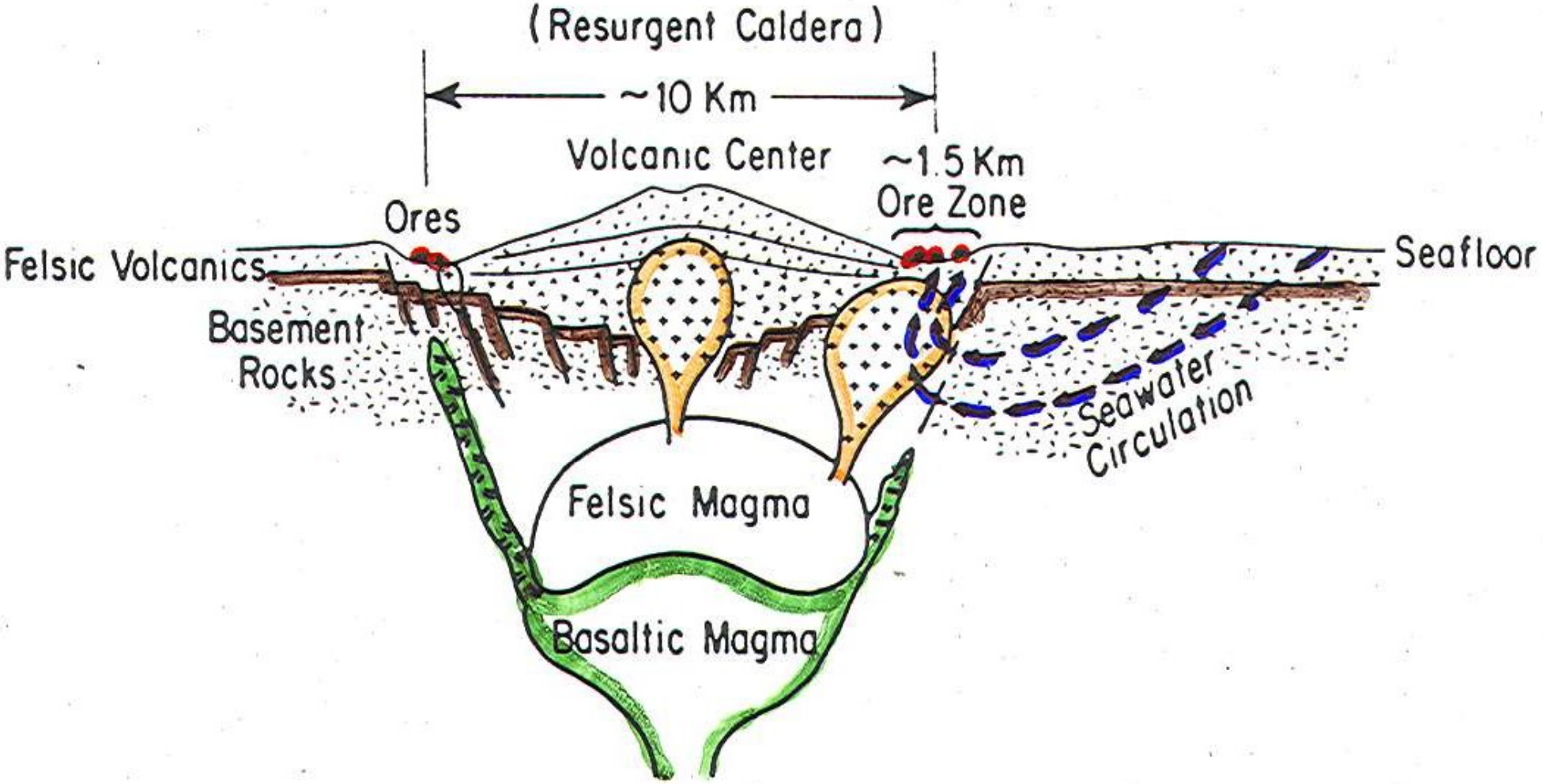
(Resurgent Caldera)
~10 Km
Volcanic Center
~1.5 Km
Ore Zone
Ores
Felsic Volcanics
Seafloor
Basement
Rocks
Seawater
Circulation
Felsic Magma
Basaltic Magma

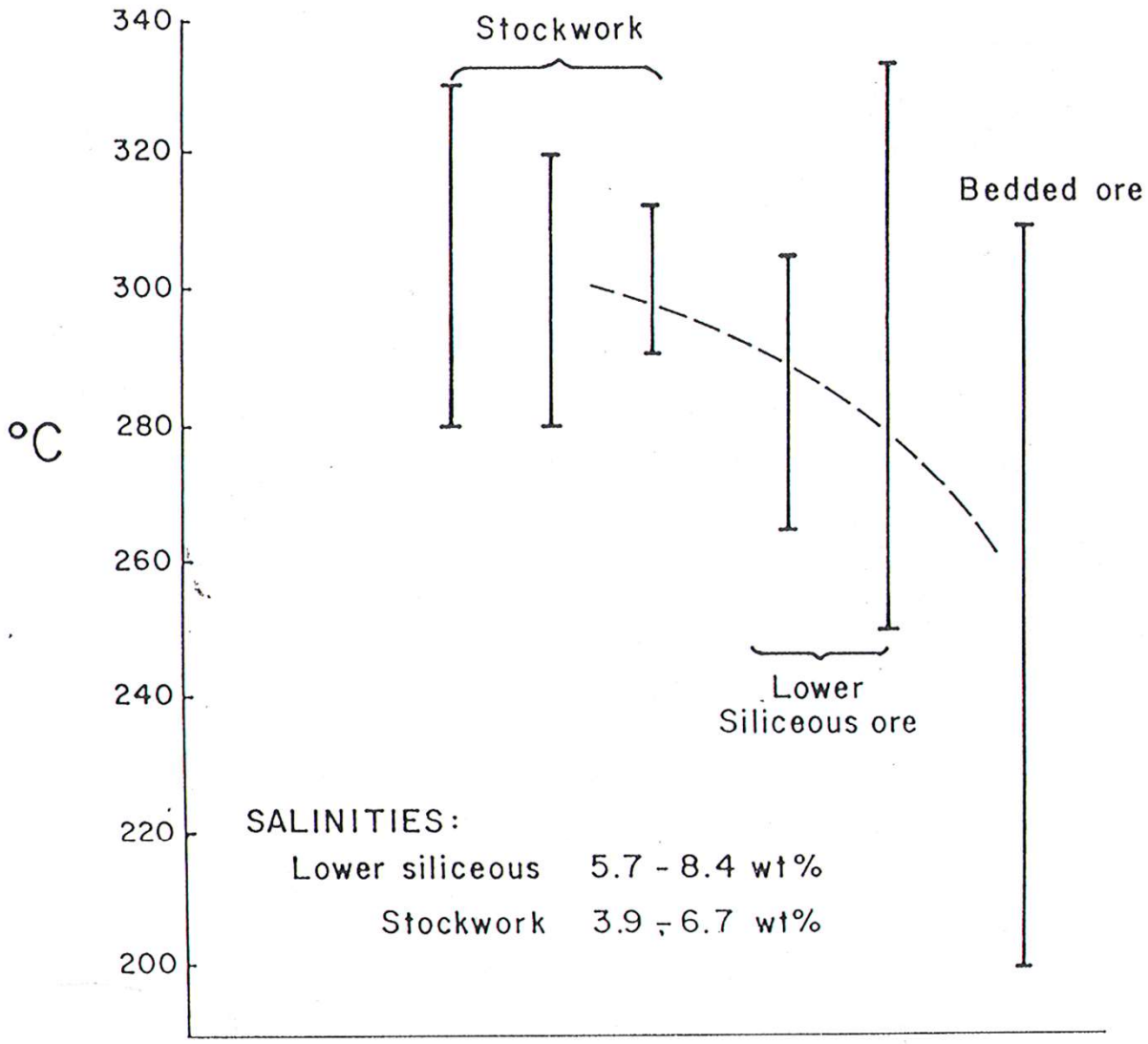

Compilation of representative fluid inclusion data available for Kuroko deposits

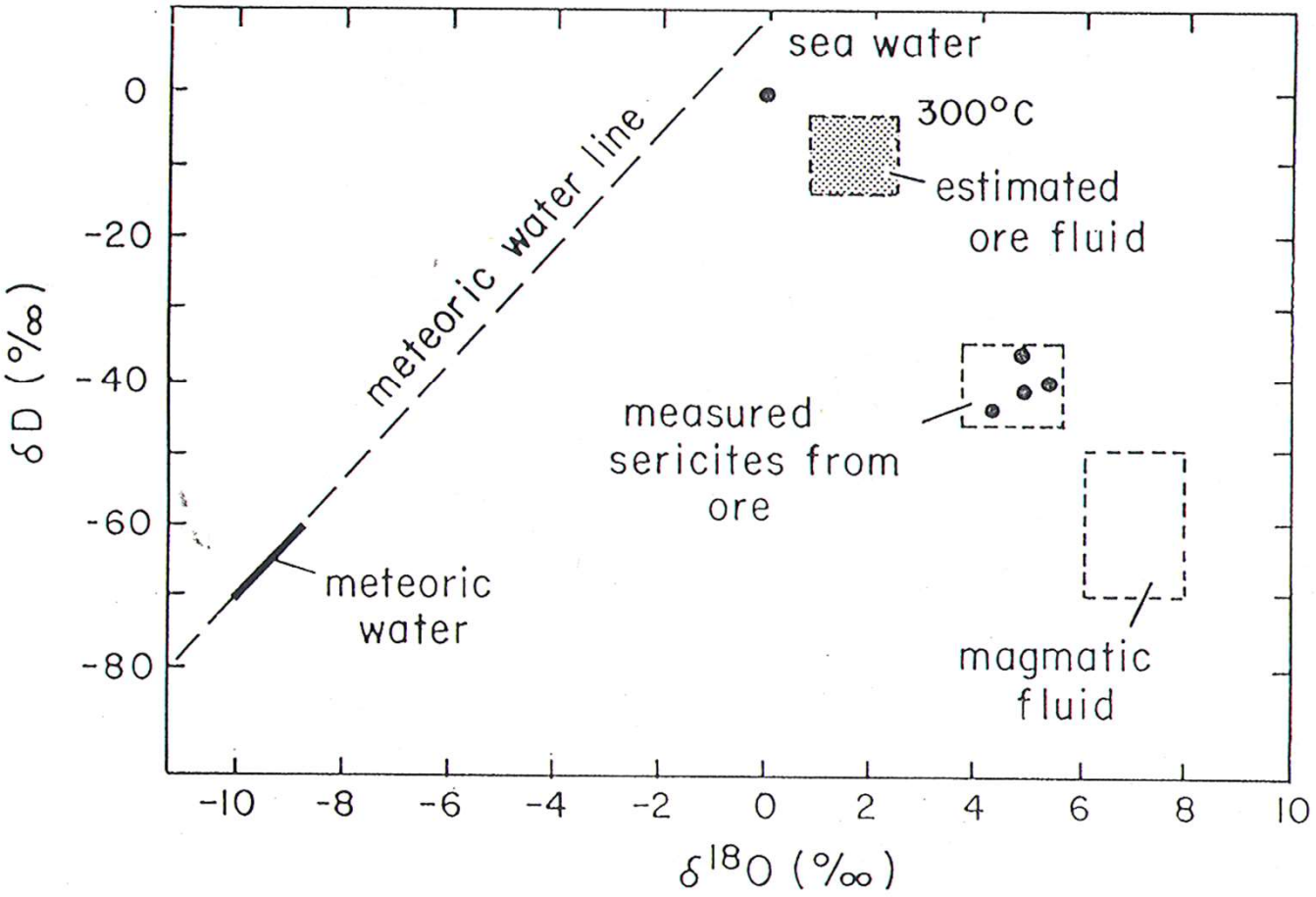

Plot of ^{18}O vs D data pertinent to Kuroko ore fluids. These data, although not unequivocal, provide strong support for a genetic model involving a certain contribution of magmatic water to Kuroko ore fluids (from Hattori and Muehlenbachs, 1980)

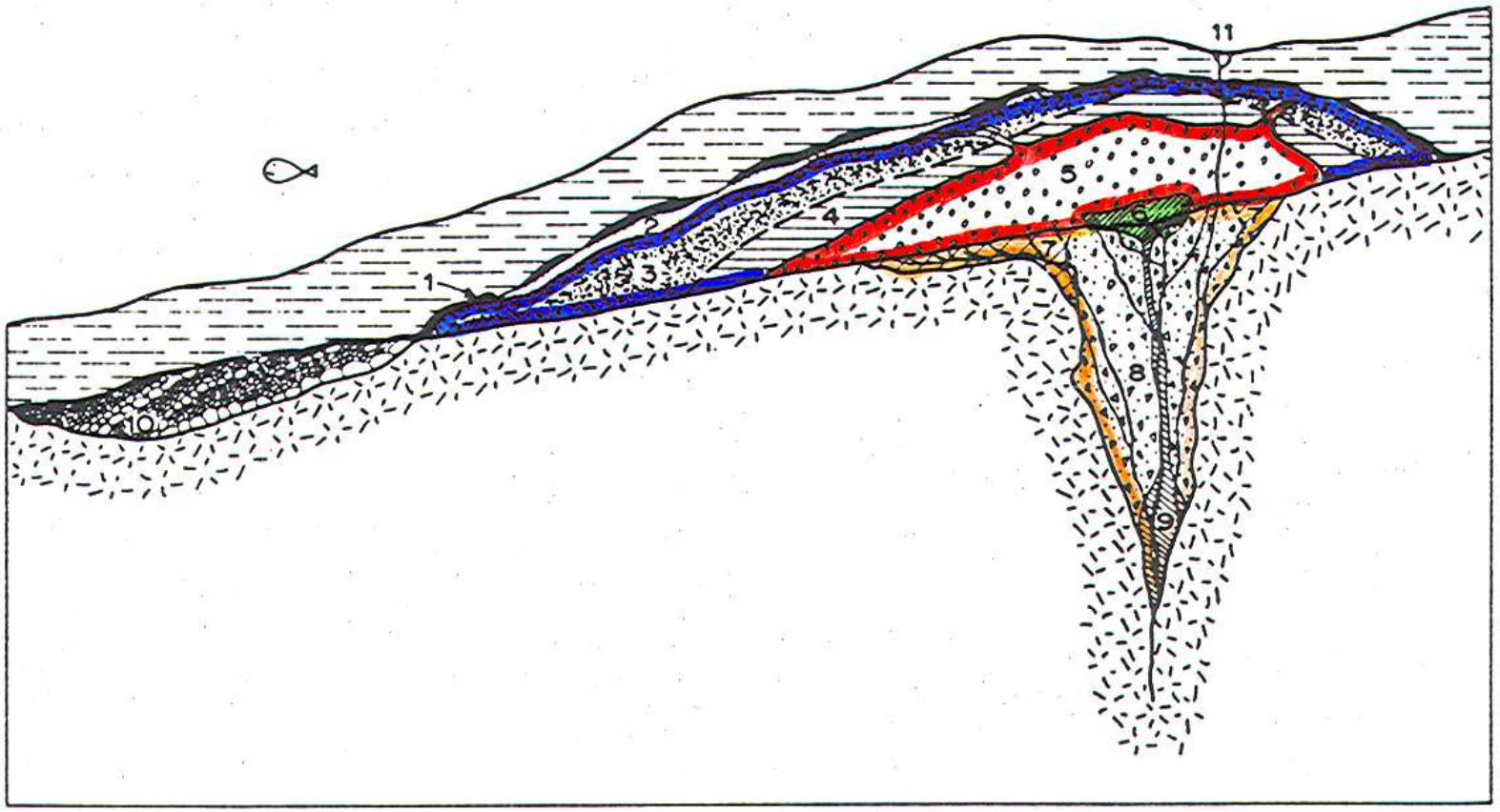

An idealized representation of a relatively undisturbed Kuroko deposit. 1 = tetsusekiei or chert-hematite layer, 2 = barite ore, 3 = massive black ore (sphalerite + pyrite + galena + barite) where the fine dotted line separates the overlying fine-grained ore from the coarser grained ore below, 4 = massive semiblack ore (sphalerite + pyrite + chalcopyrite), 5 = massive yellow ore (chalcopyrite + pyrite), 6 = massive pyrite ore (pyrite + quartz), 7 = siliceous black ore (sphalerite + pyrite + galena + quartz) 8 = siliceous yellow ore (chalcopyrite + pyrite + quartz), 9 = siliceous pyrite ore (pyrite + quartz), 10 = transported, fragmental massive ore (mostly black), 11 = late-stage sulfide veins which can be either black or yellow ore. Though gypsum ore is often present underneath and peripheral to massive ores, we did not examine any in this study and have chosen to delete it for the sake of simplicity.

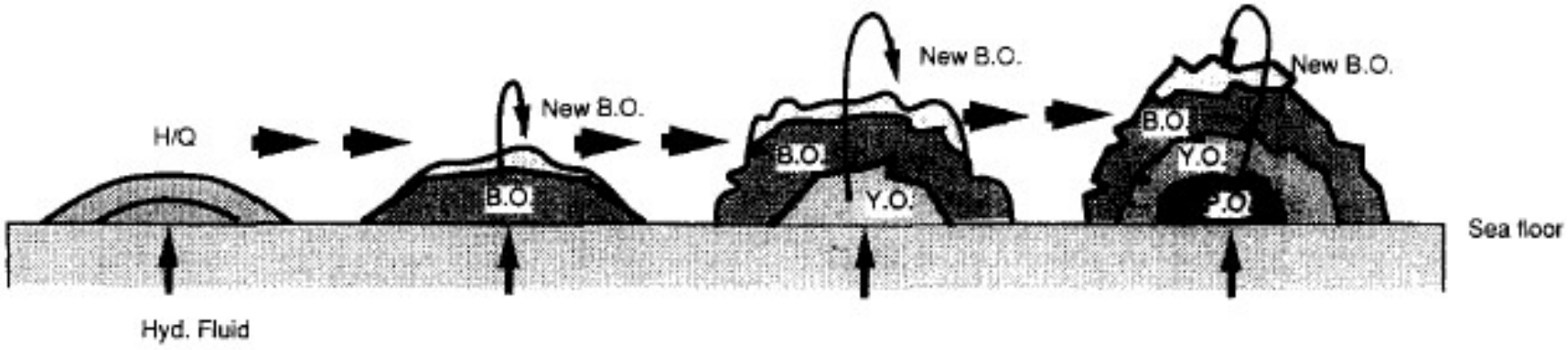
H/Q
New B.O.
New B.O.
New B.O.
B.O.
B.O.
Y.O.
B.O.
Y.O.
P.O.
Sea floor
Hyd. Fluid

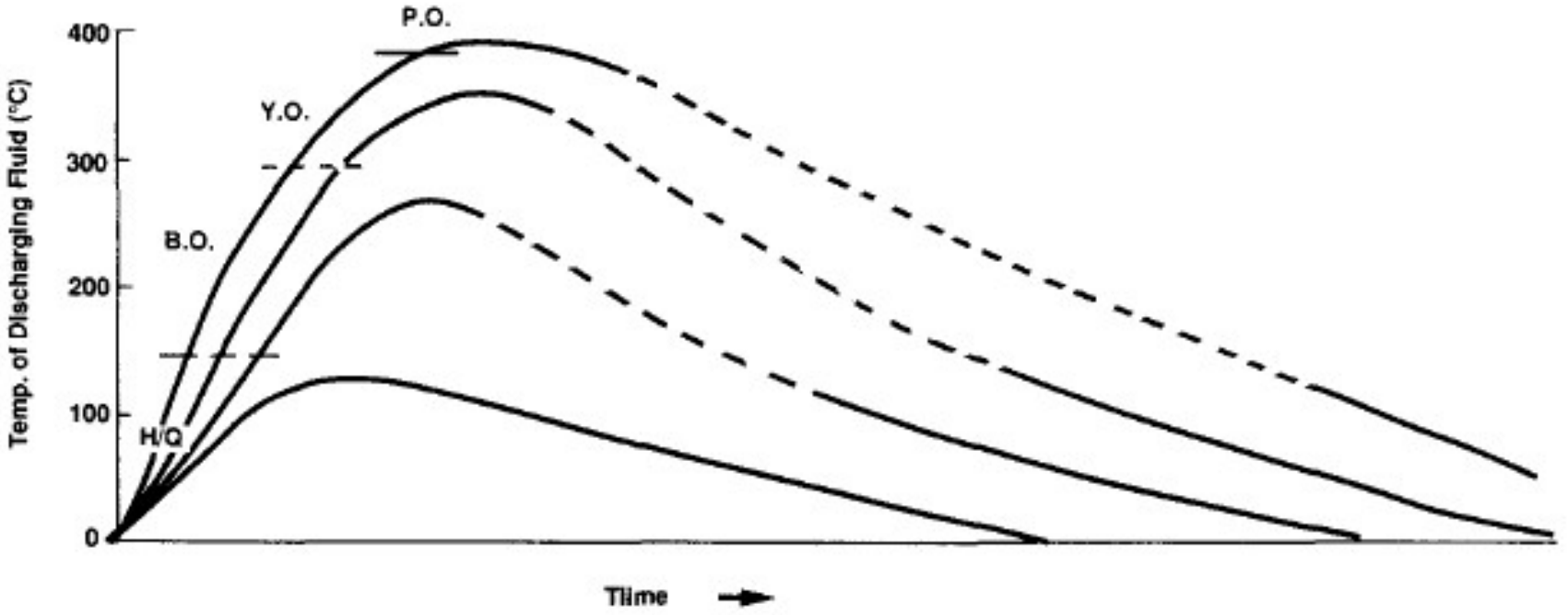
P.O.
Y.O.
B.O.
H/Q
400
300
200
100
0
Temp. of Discharging Fluid (°C)
Time

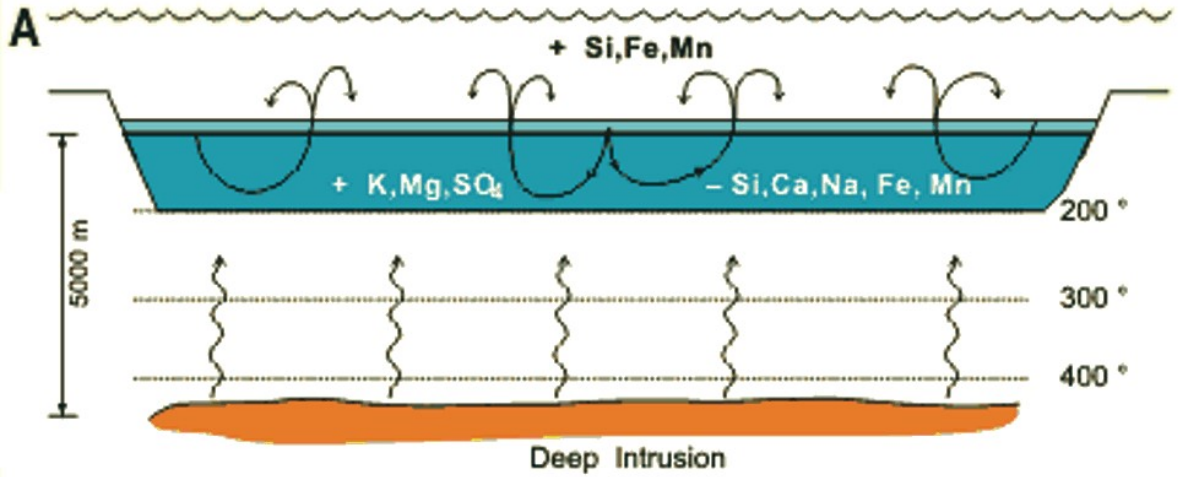
A
+ Si,Fe,Mn
+ K,Mg,SO4
– Si,Ca,Na, Fe, Mn
5000 m
200 °
300 °
400 °
Deep Intrusion
SHALLOW CONVECTION

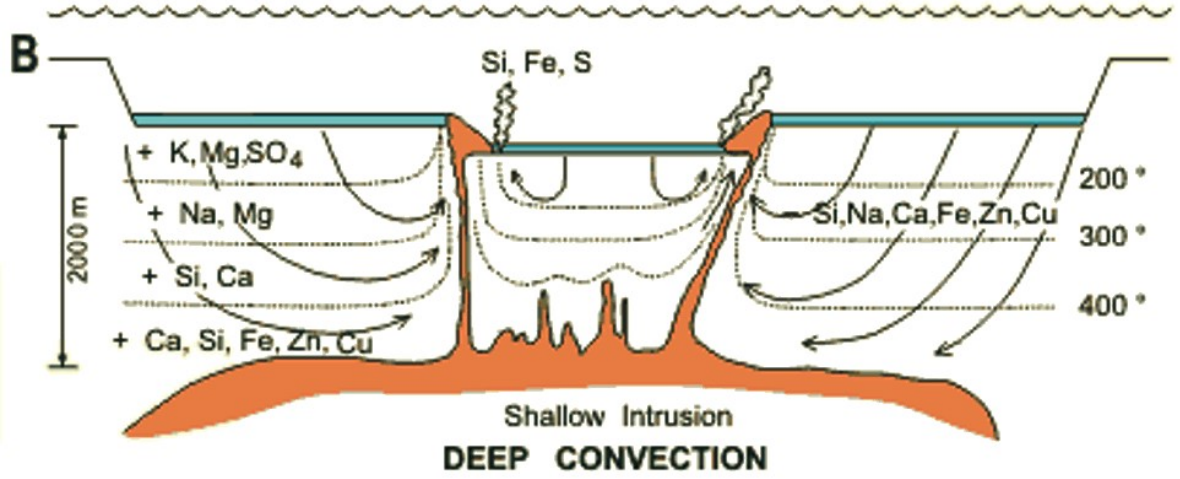
B
Si, Fe, S
+ K,Mg,SO4
+ Na, Mg
+ Si, Ca
+ Ca, Si, Fe, Zn, Cu
2000 m
Si,Na,Ca,Fe,Zn,Cu
200 °
300 °
400 °
Shallow Intrusion
DEEP CONVECTION

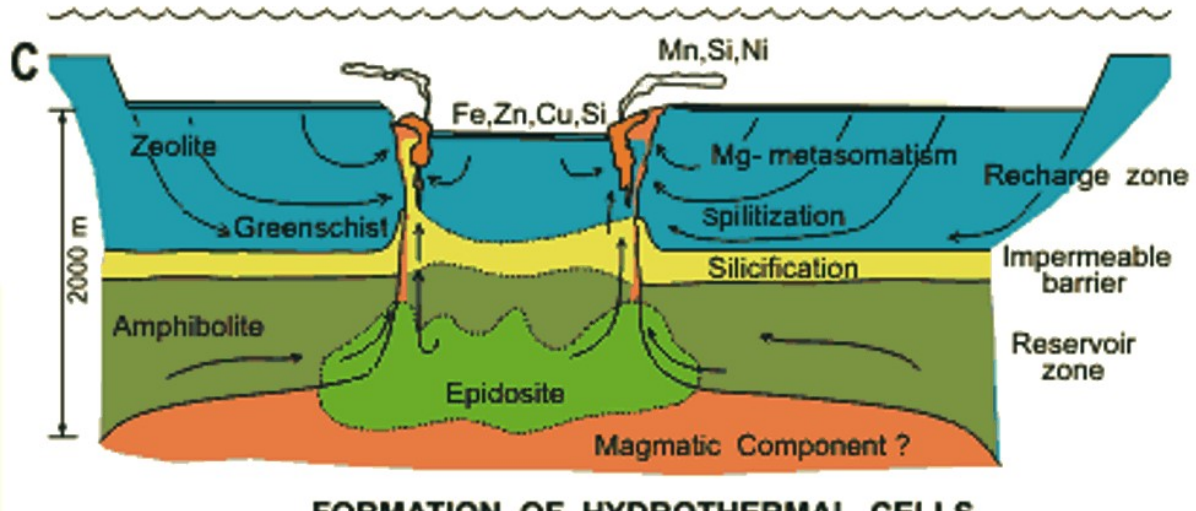
C
Mn,Si,Ni
Fe,Zn,Cu,Si
Zeolite
Greenschist
Mg- metasomatism
Spilitization
Recharge zone
Silicification
Impermeable barrier
Amphibolite
Reservoir zone
Epidosite
Magmatic Component ?
2000 m
FORMATION OF HYDROTHERMAL CELLS

Some reactions involving the alteration of basalt to hydrous secondary mineral assemblages. The concentration of trace metal in the product solution is calculated assuming that a total of 50 ppm trace metal is lost from the weight of basalt which reacts with the solution. The minimum seawater:basalt ratio is calculated from the weight of seawater (containing 1350 ppm Mg) required to supply the weight of magnesium and/or water required to supply the reactants.

REACTION 1

$0.076\ \text{Basalt} + 0.963\ Mg^{2+} + 2.212\ H_2O + 0.084\ O_2 \rightarrow 1.00\ \text{Smectite} + 0.785\ Ca^{2+} + 0.202\ Na^{+} + 0.024\ Fe^{2+} + 0.088\ H^{+} + 0.587\ H_4SiO_4$

Minimum seawater : basalt ratio = 42:1

< 1 ppm trace metal in product solution

REACTION 2

$0.104\ \text{Basalt} + 0.663\ Mg^{2+} + 0.155\ Na^{+} + 1.781\ H^{+} + 1.187\ H_2O + 0.149\ O_2 \rightarrow 1.00\ \text{Smectite} + 0.50\ \text{Albite} + 1.260\ Ca^{2+} + 0.326\ Fe^{2+} + 0.525\ H_4SiO_4$

Minimum seawater : basalt ratio = 20:1

< 2 ppm trace metal in product solution

REACTION 3

$1.000\ \text{Basalt} + 0.009\ Mg^{2+} + 10.379\ H_2O + 0.179\ O_2 \rightarrow 4.90\ \text{Albite} + 1.604\ \text{Chlorite} + 2.075\ \text{Actinolite} + 3.776\ \text{Epidote} + 1.893\ \text{Quartz} + 0.009\ Ca^{2+}$

Minimum seawater : basalt ratio = 1:30

> 1500 ppm trace metal in product solution

MINERAL FORMULAE

Smectite: $(Na_{.17}\ Ca_{.09}Mg_{1.73}Fe^{2+}_{.32}Fe^{3+}_{.43}Al_{.39})(Al_{.90}Si_{3.10})O_{10}(OH)_2$ (Seyfried and Bischoff, 1977)

Chlorite: $(Mg_{.51}Fe_{.49})_5\ Al_2Si_3O_{10}\ (OH)_8$

Actinolite: $Ca_{2.0}\ (Mg_{.60}Fe_{.40})_5\ Si_{8.0}O_{22}\ (OH)_2$

Epidote: $Ca_{2.0}\ (Fe_{.60}Al_{2.40})\ Si_3O_{12}\ (OH)$

Albite: $Na\ Al\ Si_3\ O_8$

Approximate average compositions in altered ocean floor basalts (Humphris and Thomson, 1978).

Basalt: $Na_{4.90}(Ca_{11.71}Mg_{10.27}Fe^{2+}_{8.83}Fe^{3+}_{1.55})\ Al_{17.18}Si_{49.33}O_{160}$ Barth unit cell from analysis by Seyfried and Bischoff, 1977

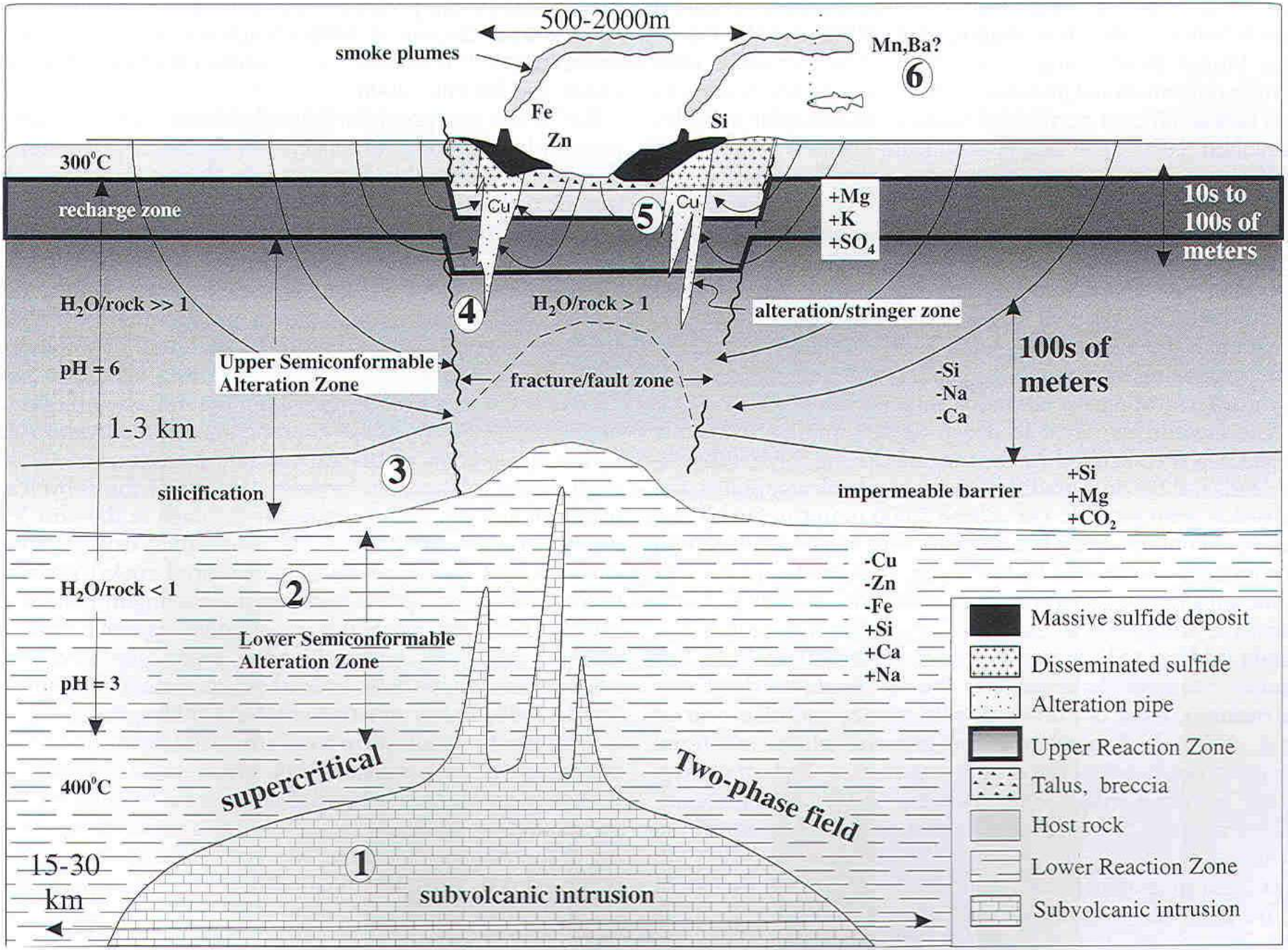

General model for the formation of VMS deposits, illustrating the basic components of a high-temperature VMS hydrothermal system (after Galley, 1993; Franklin, 1995). Note variable horizontal and vertical scales. See text for numbers.

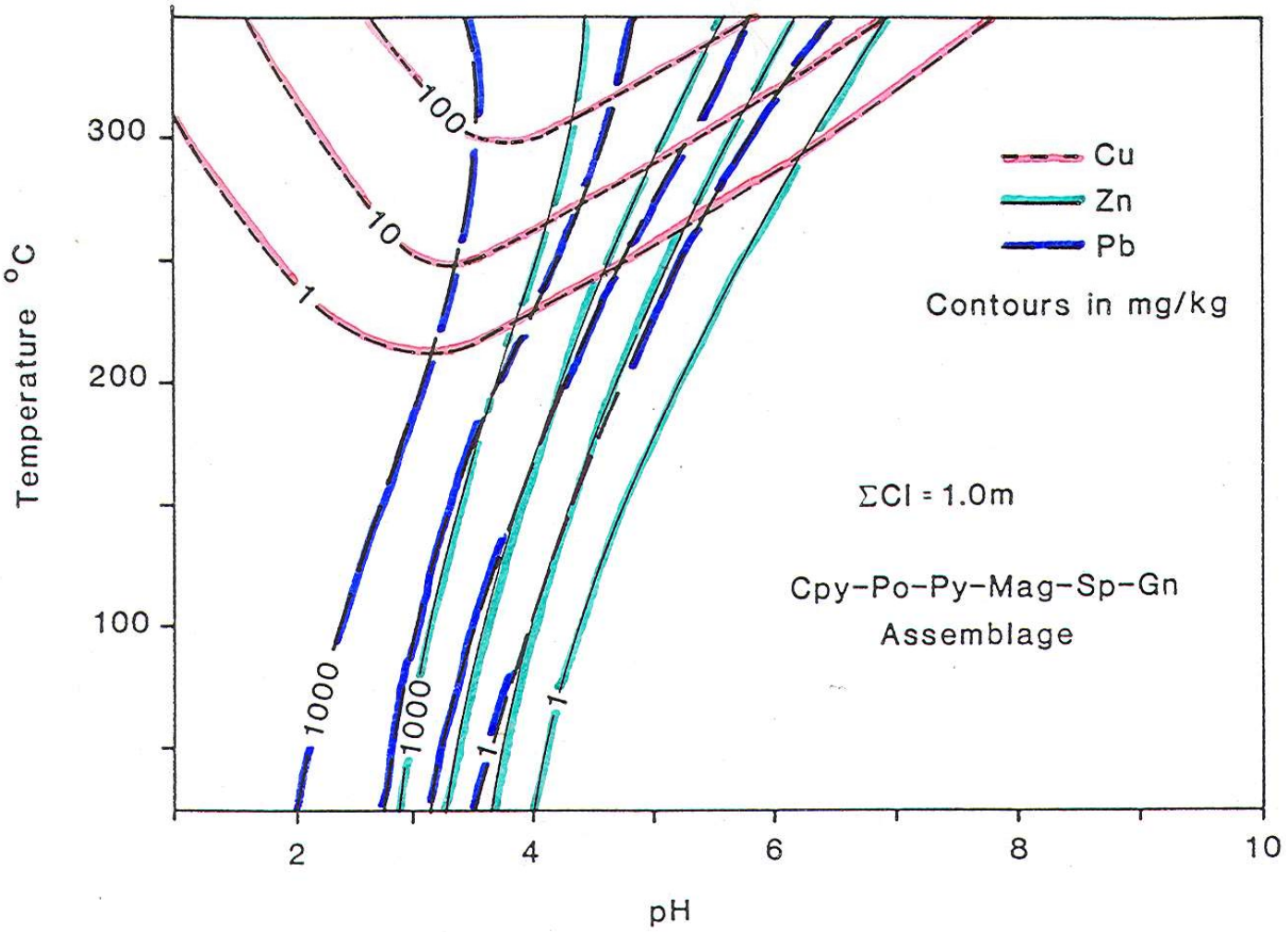

Sulphide solubility patterns due to chloride complexing. Calculated total metal concentrations (in $mg \cdot kg^{-1}$*) in a 1 m NaCl solution in equilibrium with a chalcopyrite-pyrite-pyrrhotite-magnetite-sphalerite-galena assemblage. Note that the sulphur content of the solution ranges from tt* $1\ mg \cdot kg^{-1}$ *at low pH and low temperature to* $>$ $10{,}000\ mg \cdot kg^{-1}$ *at high pH and high temperature. The isothermal decrease in chalcopyrite solubility with decreasing pH at low pH is due to the decrease in activity of* Cl^- *as the relative proportion of chloride complexed with metals increases. (Data from Helgeson, 1969; and Crerar and Barnes, 1976).*

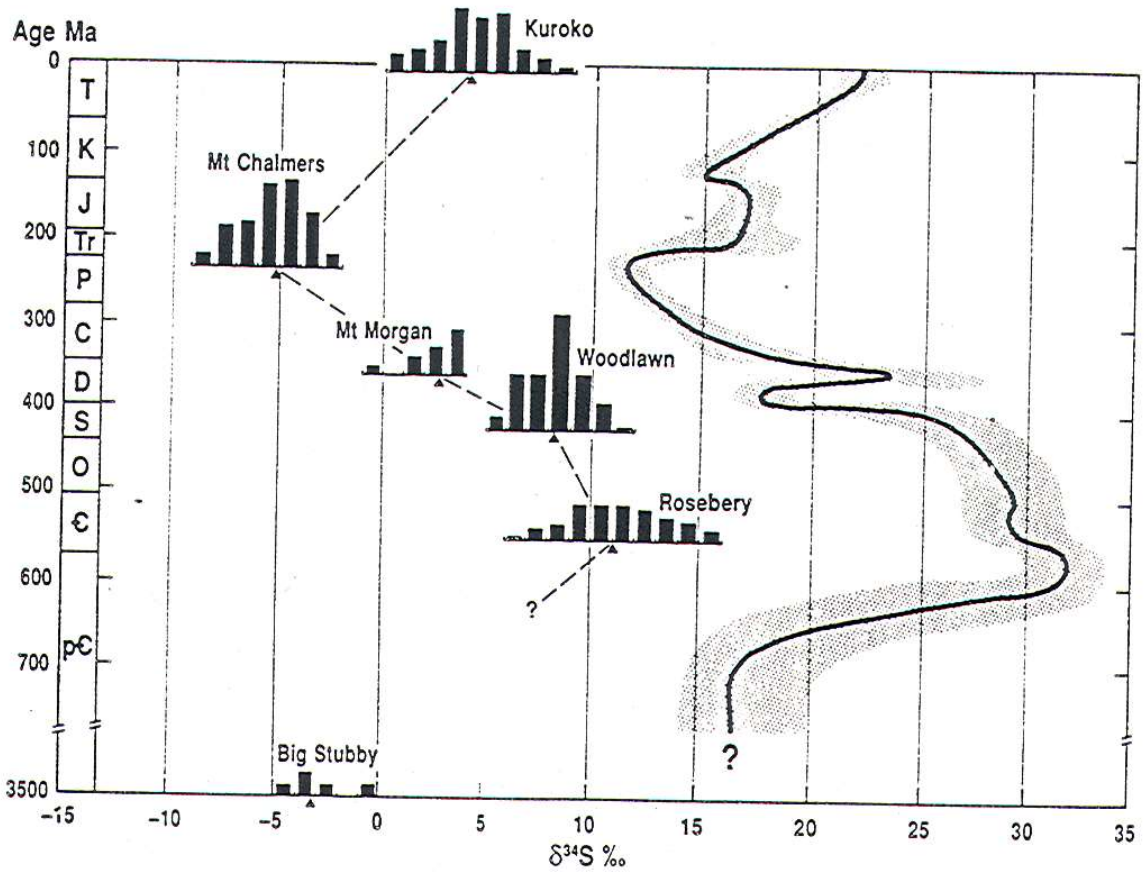

Sulfur isotope composition of ore sulfides (pyrite, sphalerite, chalcopyrite) from some major Australian VHMS deposits and the kuroko deposit from the Hokuroko district, Japan, compared with the age curve for marine sulfate from Claypool et al. (1980). Sources of data are Kuroko (Ohmoto et al., 1983), Mount Chalmers (Both and Large, unpub. data), Mount Morgan (Eadington et al., 1974), Woodlawn (Ayres et al., 1979), Rosebery (Green et al., 1981; Khin Zaw, 1991), and Big Stubby (Lambert et al., 1978).

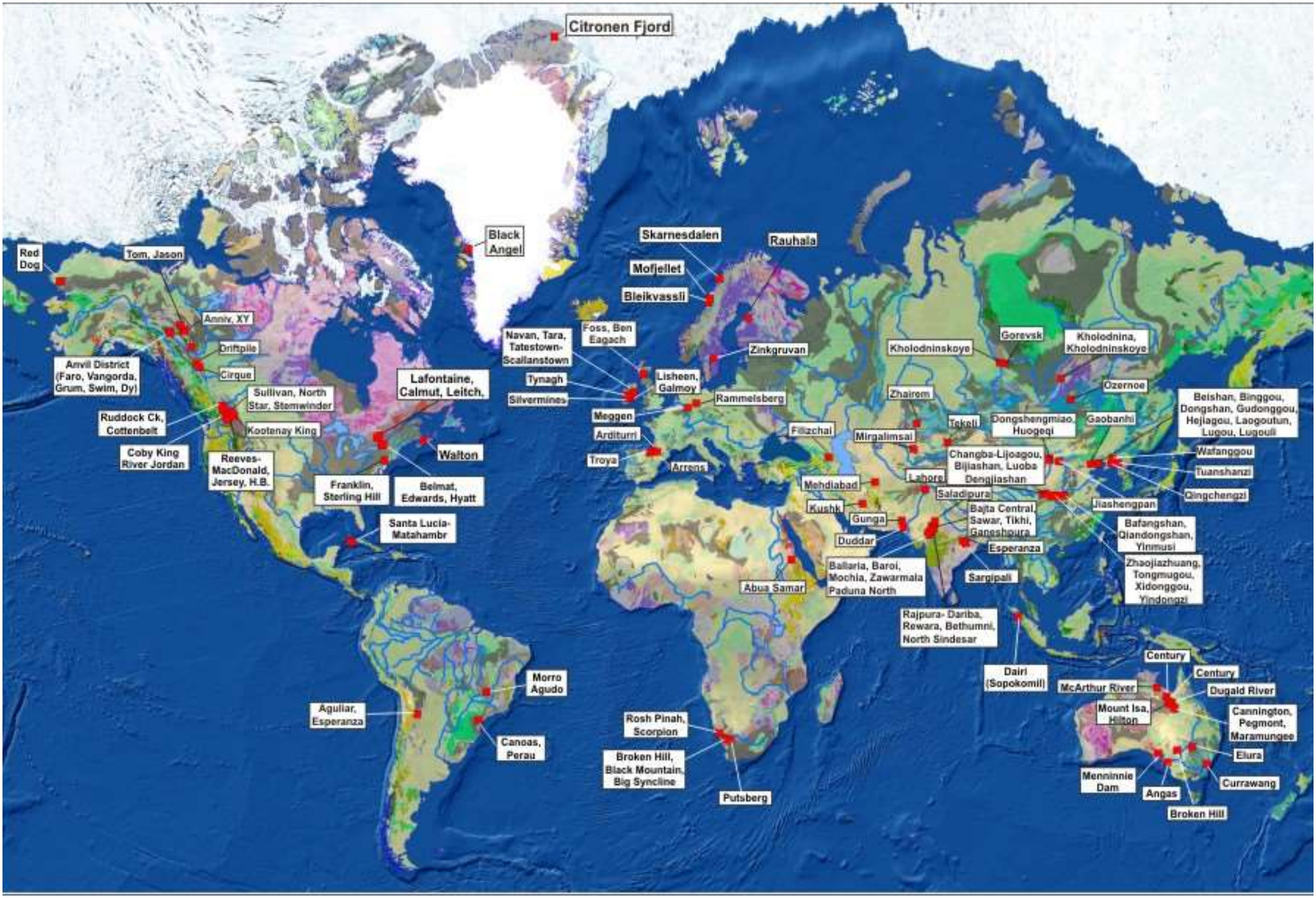
Citronen Fjord
Black Angel
Red Dog
Tom, Jason
Anniv, XY
Driftpile
Cirque
Anvil District (Faro, Vangorda, Grum, Swim, Dy)
Sullivan, North Star, Sternwinder
Ruddock Ck, Cottenbelt
Kootenay King
Coby King River Jordan
Reeves-MacDonald, Jersey, H.B.
Lafontaine, Calmut, Leitch,
Walton
Belmat, Edwards, Hyatt
Franklin, Sterling Hill
Santa Lucia-Matahambr
Morro Agudo
Aguilar, Esperanza
Canoas, Perau
Skarnesdalen
Mofjellet
Bleikvassli
Rauhala
Navan, Tara, Tatestown-Scallanstown
Foss, Ben Eagach
Tynagh
Silvermines
Lisheen, Galmoy
Meggen
Arditurri
Troya
Arrens
Rammelsberg
Zinkgruvan
Rosh Pinah, Scorpion
Broken Hill, Black Mountain, Big Syncline
Putsberg
Abua Samar
Mehdiabad
Kushk
Gunga
Duddar
Ballaria, Baroi, Mochia, Zawarmala Paduna North
Rajpura- Dariba, Rewara, Bethumni, North Sindesar
Sargipali
Esperanza
Bajta Central, Sawar, Tikhi, Ganeshpura
Saladipura
Lahore
Changba-Lijoagou, Bijiashan, Luoba Dengjiashan
Mirgalimsai
Felizchai
Zhairem
Tekeli
Kholodninskoye
Kholodnina, Kholodninskoye
Gorevsk
Ozernoe
Dongshengmiao, Huogeqi
Gaobanhi
Beishan, Binggou, Dongshan, Gudonggou, Hejiagou, Laogoutun, Lugou, Lugouli
Wafanggou
Tuanshanzi
Qingchengzi
Jiashengpan
Bafangshan, Qiandongshan, Yinmusi
Zhaojiazhuang, Tongmugou, Xidonggou, Yindonggi
Dairi (Sopokomil)
Century
Century
McArthur River
Dugald River
Mount Isa, Hilton
Cannington, Pegmont, Maramungee
Elura
Currawang
Broken Hill
Angas
Menninnie Dam

STRATIGRAPHIC FEATURES OF FIVE GIANT, PROTEROZOIC, SEDIMENT-HOSTED LEAD-ZINC DEPOSITS

Deposit	Contained metal (10^6 tons)	Underlying section: Thickness (km)	Underlying section: Lithologies	Mineralized section: Thickness (m)	Mineralized section: No. ore lenses	Interore lithologies	References
Mount Isa, Queensland, Australia	6.3 Pb 5.4 Zn	6	Fine-grained clastics and carbonates; shallow marine (lacustrine?) with minor evaporites	650	28	Dolomitic shales and siltstones; thin tuffs	Mathias and Clark (1975)
Hilton, Queensland, Australia	2.7 Pb 3.4 Zn	6	Same as above	150	7	Same as above	Mathias et al. (1971)
H.Y.C., Northern Territories, Australia	9.7 Pb 21.8 Zn	7	Sandstone, shale, dolomite, and abundant evaporitic units	130	7	Pyritic and dolomitic shales, slump breccias; thin tuffs	Walker et al. (1977)
Sullivan, British Columbia, Canada	10.2 Pb 8.8 Zn	>2	Fine-grained clastics, turbidites; carbon and pyrrhotite-rich layers	80	8	Argillites and fine-grained quartz wackes	Hamilton et al. (1983)
Broken Hill, New South Wales, Australia	20.3 Pb 17.6 Zn	Probably several	Largely metapellites and metapsammites (metavolcanics?)	50-200	5	Sillimanite gneiss (meta-argillite)	Laing et al. (1978)

NOTE: Stratigraphic data on Sullivan deposits apply mainly to eastern part of ore body.

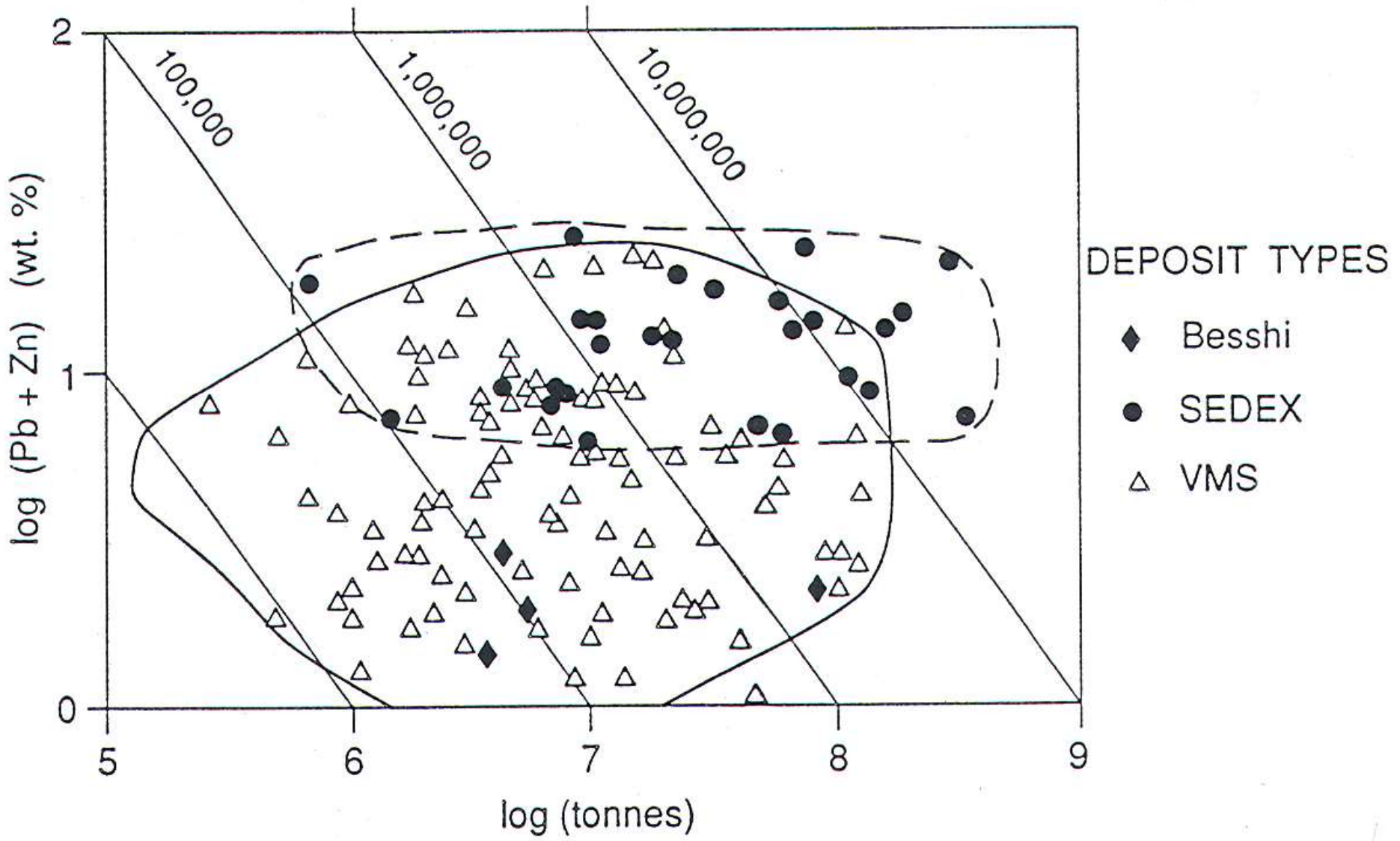
100,000
1,000,000
10,000,000
2
1
0
5
6
7
8
9
log (Pb + Zn) (wt. %)
log (tonnes)
DEPOSIT TYPES
Besshi
SEDEX
VMS

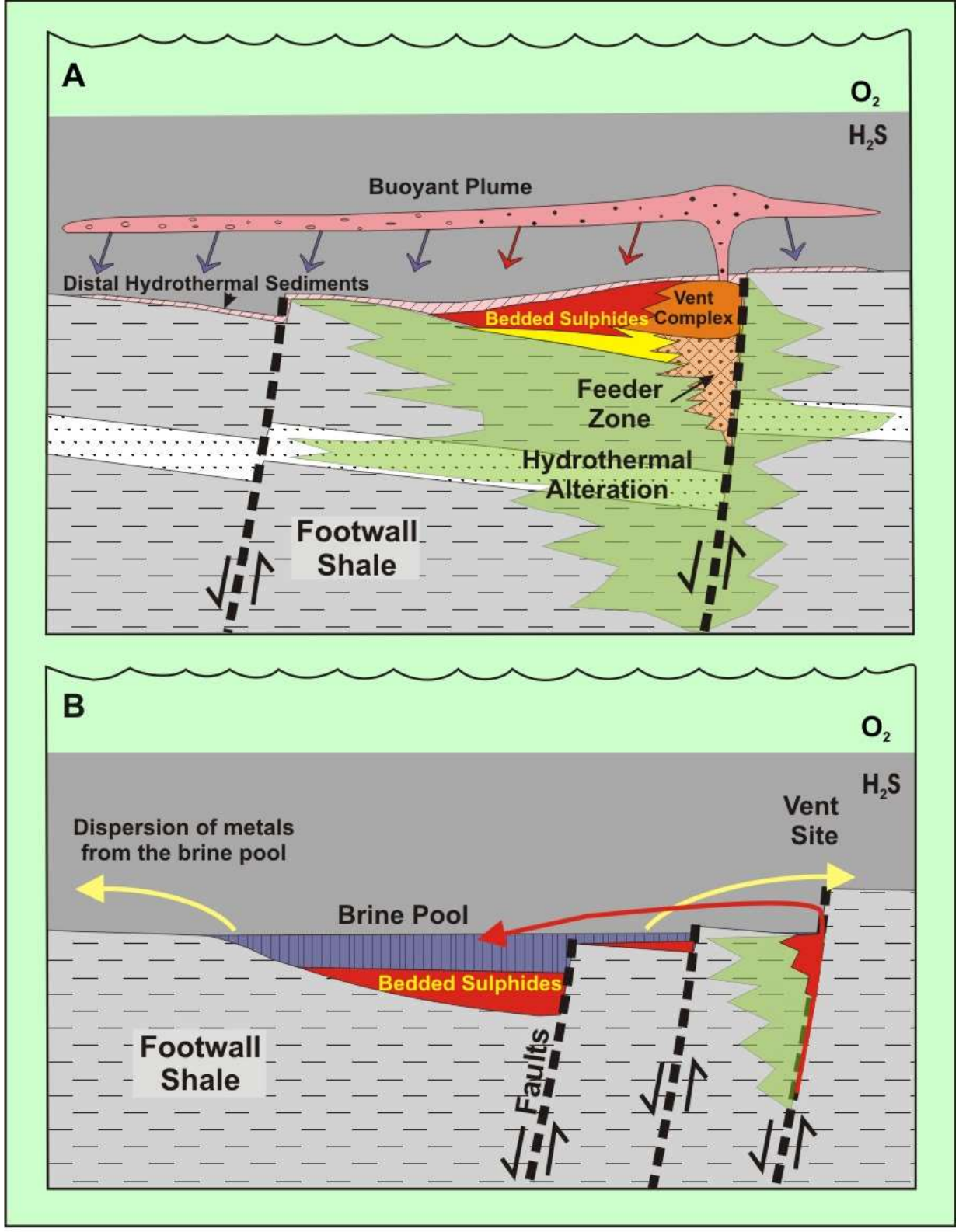
A
O_2
H_2S
Buoyant Plume
Distal Hydrothermal Sediments
Vent Complex
Bedded Sulphides
Feeder Zone
Hydrothermal Alteration
Footwall Shale
B
O_2
H_2S
Dispersion of metals from the brine pool
Vent Site
Brine Pool
Bedded Sulphides
Footwall Shale
Faults

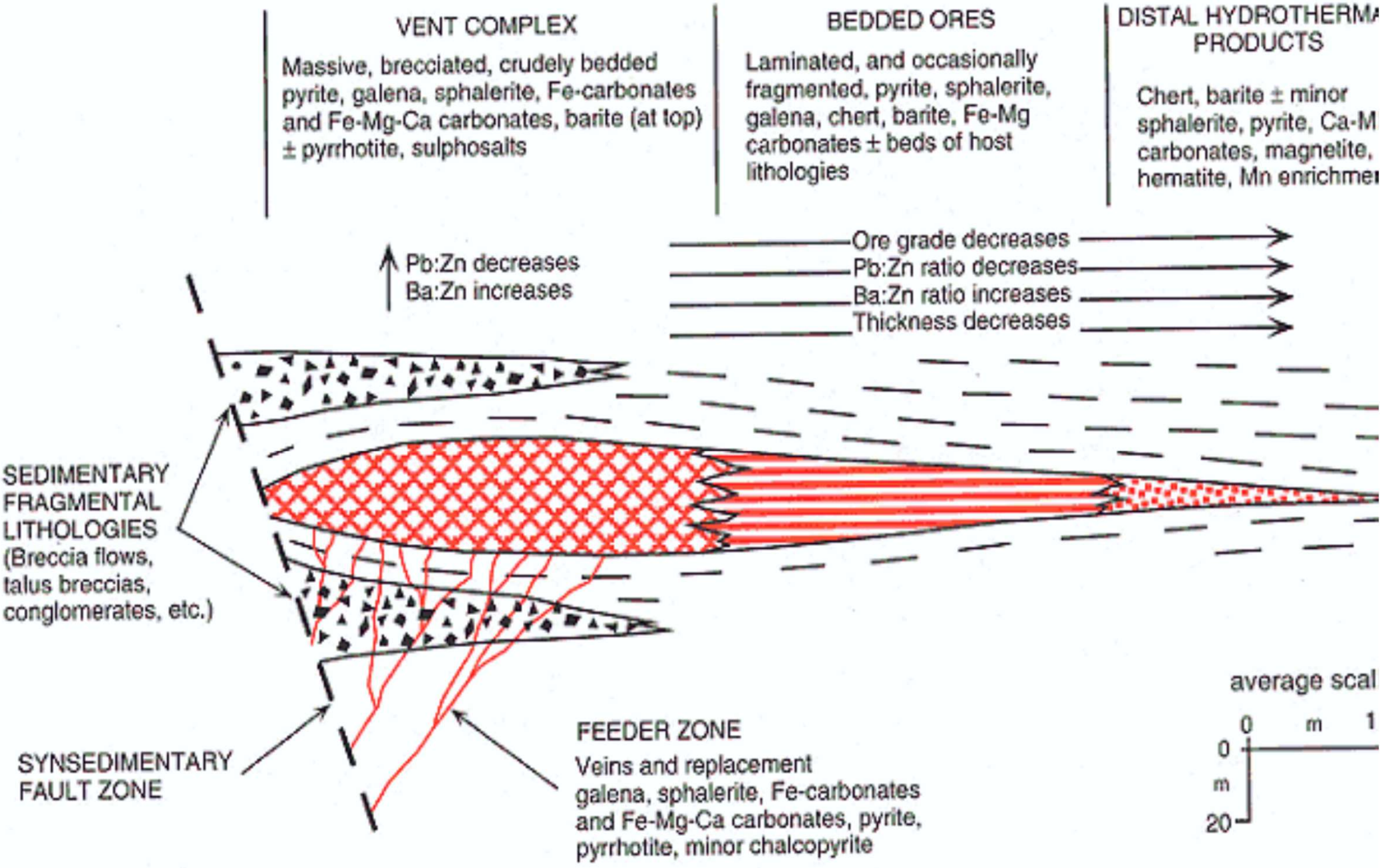

Schematic illustration of the characteristic features of the idealized Sedex deposit.

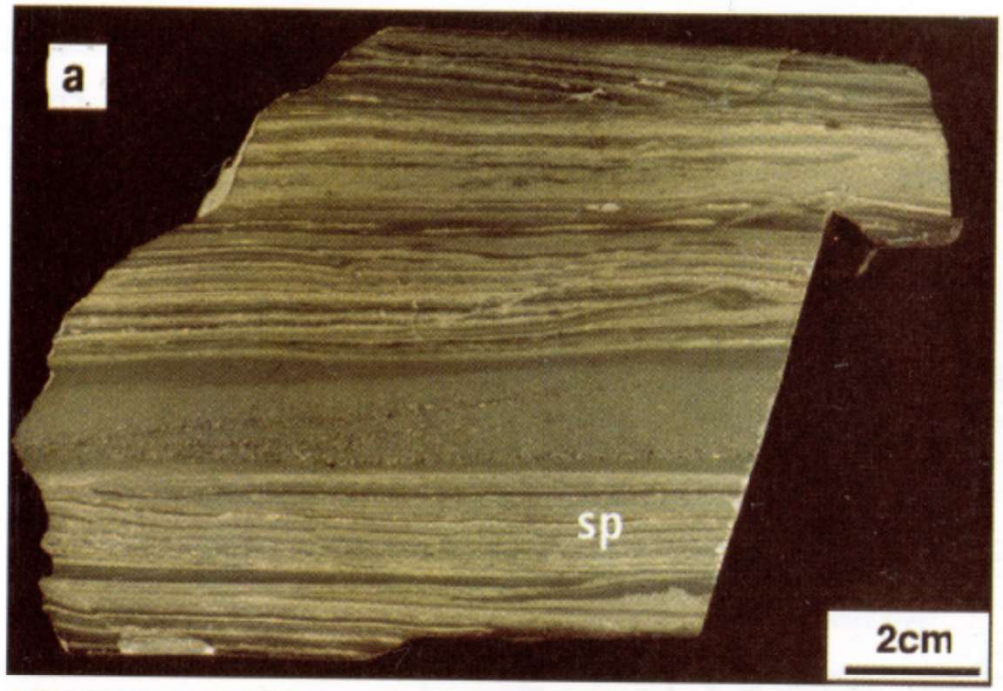
a
sp
2cm

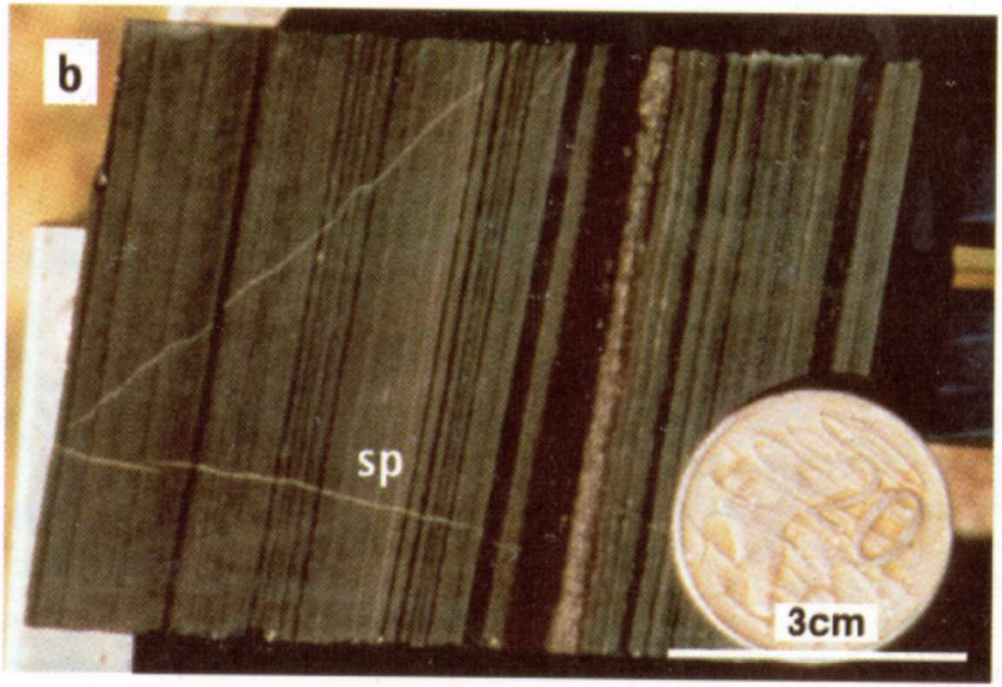
b
sp
3cm

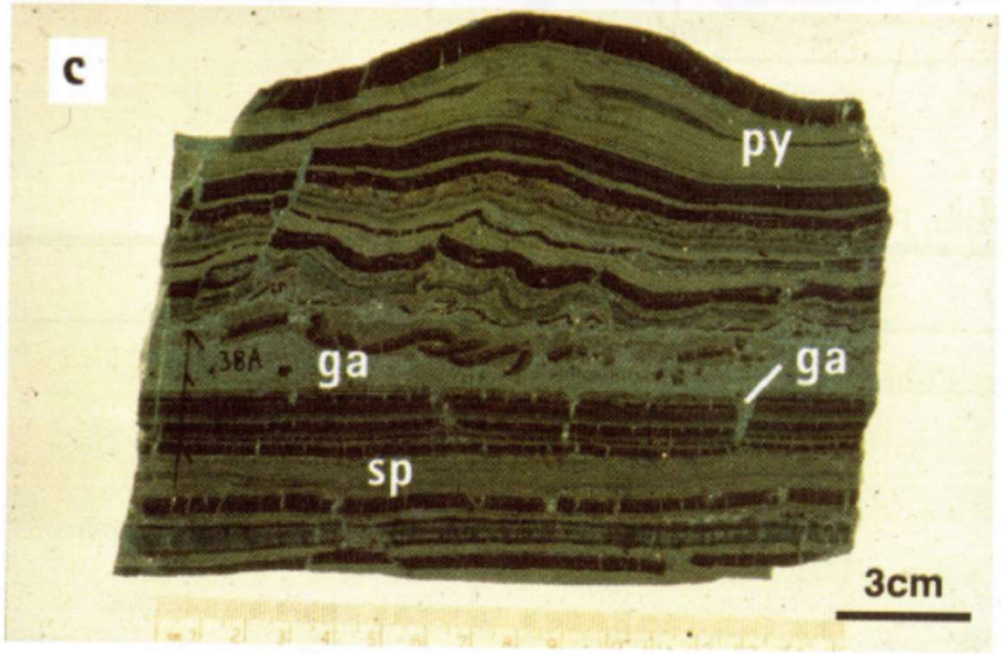
c
py
38A
ga
ga
sp
3cm

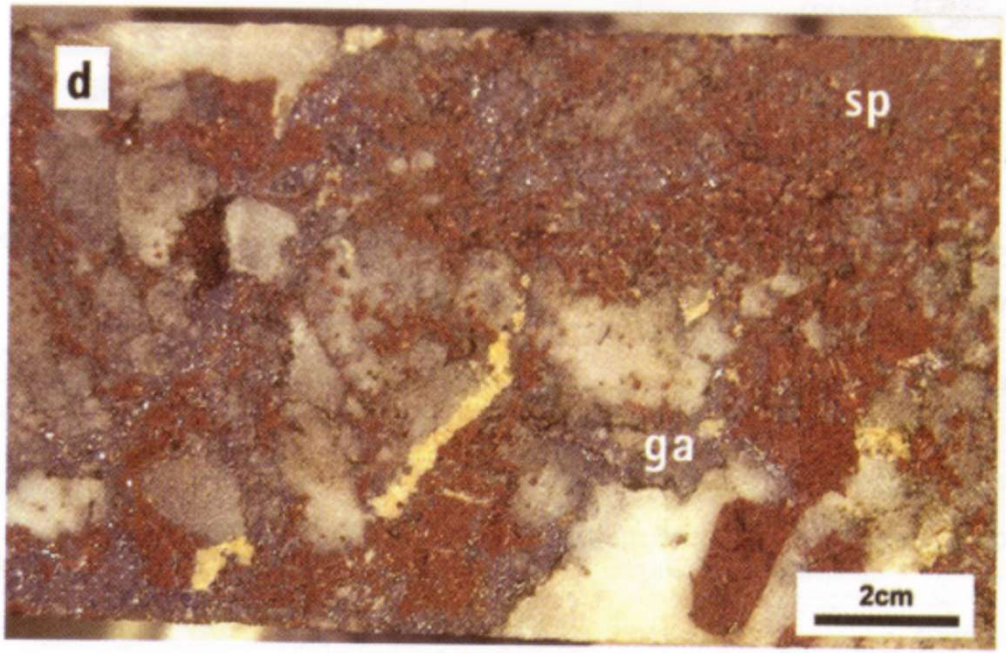
d
sp
ga
2cm

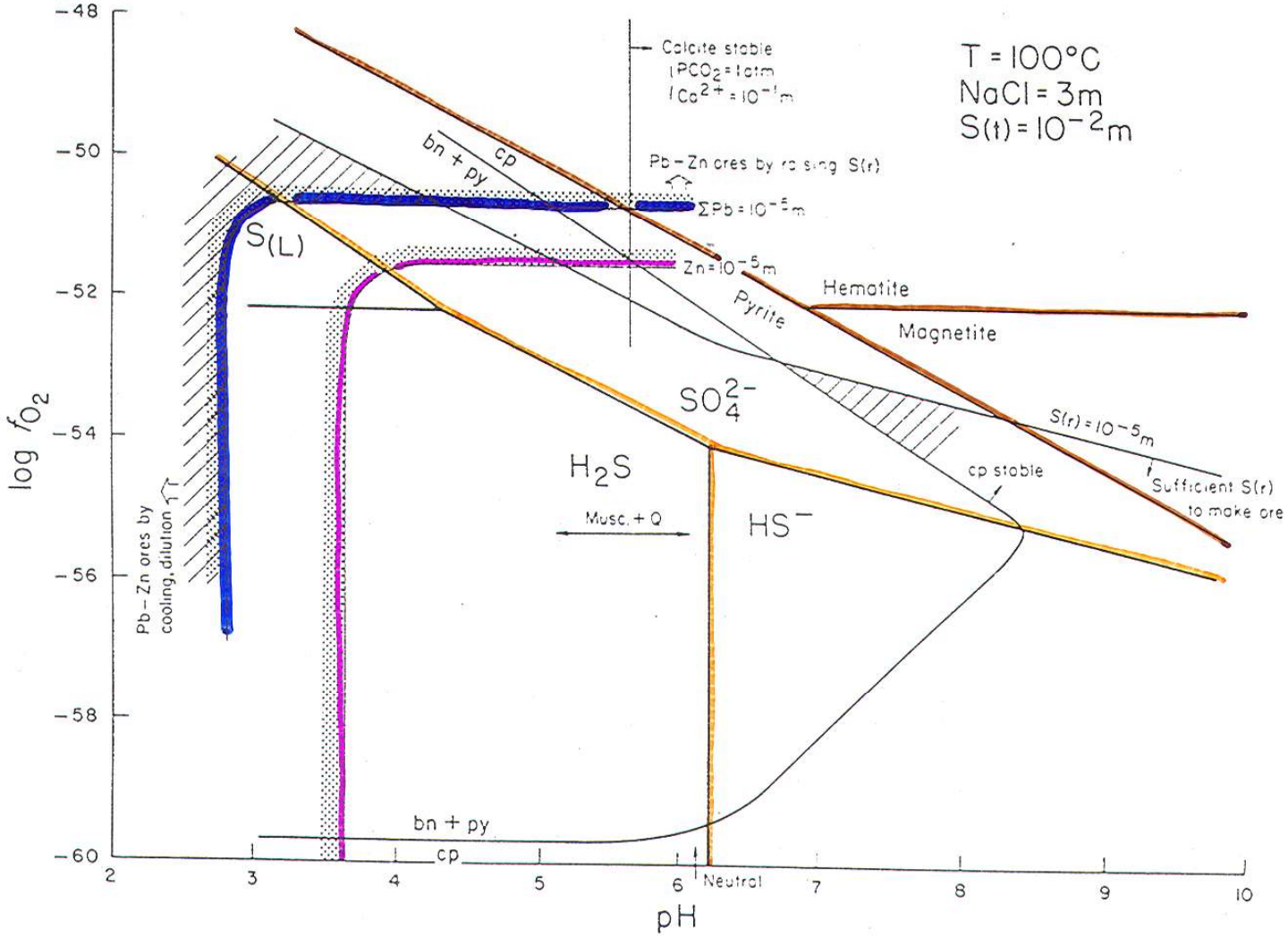
T = 100°C
NaCl = 3m
S(t) = 10⁻²m
Calcite stable
PCO2 = 1 atm
Ca2+ = 10⁻¹m
Pb–Zn ores by reducing S(r)
ΣPb = 10⁻⁵m
Zn = 10⁻⁵m
cp
bn + py
S(L)
Pyrite
Hematite
Magnetite
SO4 2−
H2S
HS⁻
Musc. + Q
S(r) = 10⁻⁵m
cp stable
Sufficient S(r) to make ore
Pb–Zn ores by cooling, dilution
bn + py
cp
Neutral
log fO2
pH
−48
−50
−52
−54
−56
−58
−60
2
3
4
5
6
7
8
9
10

Comparison of the Major Geologic and Inferred Geochemical Features of McArthur- and Selwyn-Type Deposits

	McArthur-type	Selwyn-type
Tectonic setting	Epicontinental marine platform-intracontinental rift	Epicontinental marine basin-rifted continental margin
Basin stratigraphy	Broad carbonate-evaporite platforms (shallow marine to lacustrine)	Dominated by carbonaceous siliciclastic turbidites
Basal continental rift sequence	Basal red-bed-rift tholeiite sequences	Absent
Carbonates	Commonly underlie the deposits (e.g., HYC); carbonate is also an important component in the mineralized environment	Mostly absent, rare pelagic or autochthonous carbonates at some deposits (e.g., Meggen)
Deep water conditions	Possibly local third-order sub-basins; questioned by some workers	Widespread
Relationship to volcanism	Tuffaceous horizons occur in and beneath several deposits (e.g., HYC, Mount Isa); distal felsic volcanic association, but no identified source region	Mafic to alkaline volcanics spatially and temporally associated with several deposits; possible proximal mafic volcanic association
Redox state of ore fluid	Oxidized ($SO_4^{2-} > H_2S$)	Reduced ($H_2S > SO_4^{2-}$)
Temperature	Moderate to low (<200°C)	Moderate to high (>200°C)
Salinity	High (>15 wt % NaCl)	Moderate (=10 wt % NaCl)
Pb-Zn saturation	Commonly undersaturated	Near saturation
Depositional mechanisms	Reduction, interaction with H_2S reservoir	Temperature decrease, pH increase, dilution
Vent complexes (stringer zones)	Absent	Present
Fe carbonate halo	Present	Absent (?)
Barite	Absent	Present
Gold content	<0.01 ppm	Potentially >0.1 ppm
Tin content	<2 ppm	Potentially >2 ppm

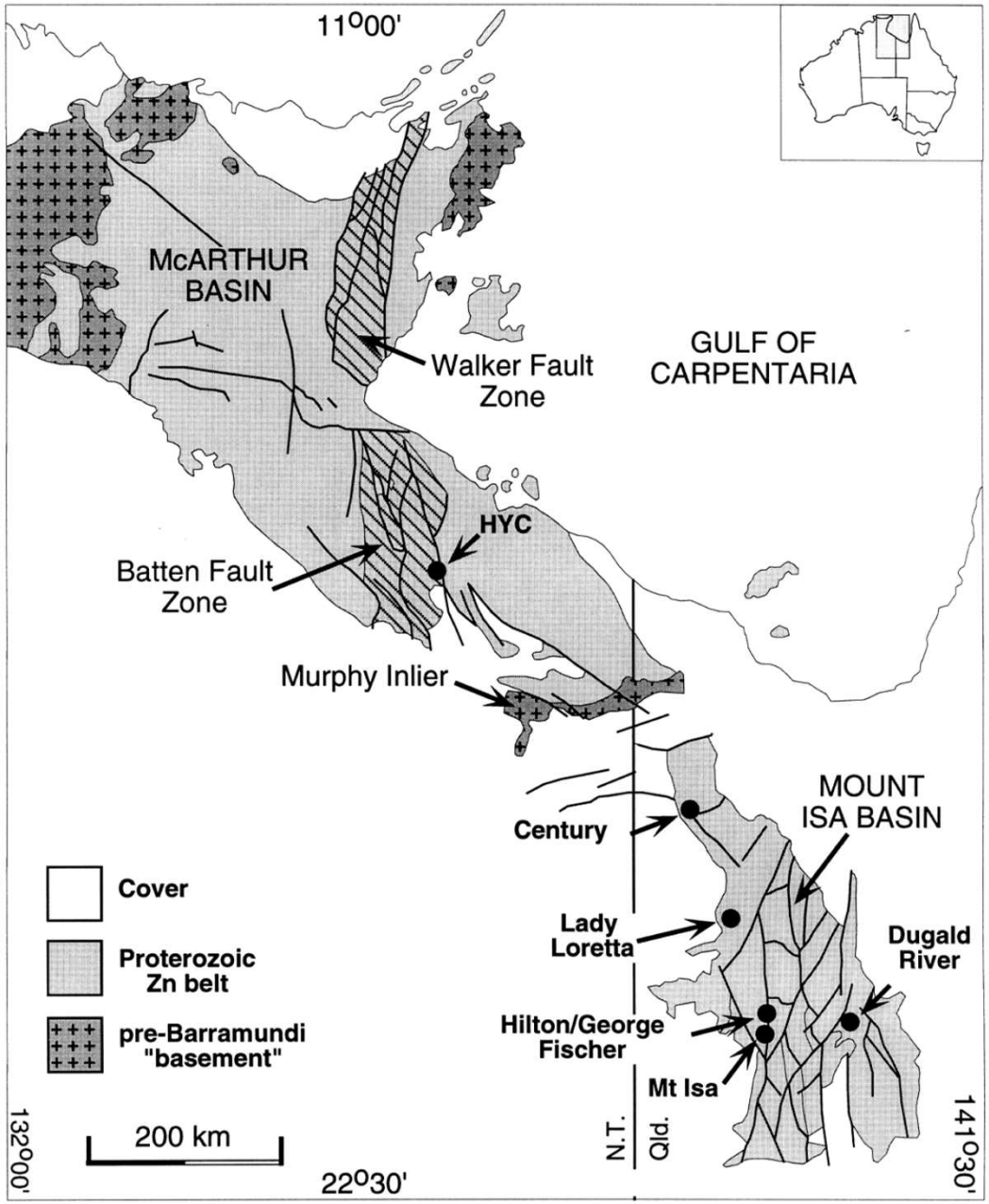

Australian Proterozoic zinc belt, showing locations of the major sedex deposits and the key geologic elements of the region.

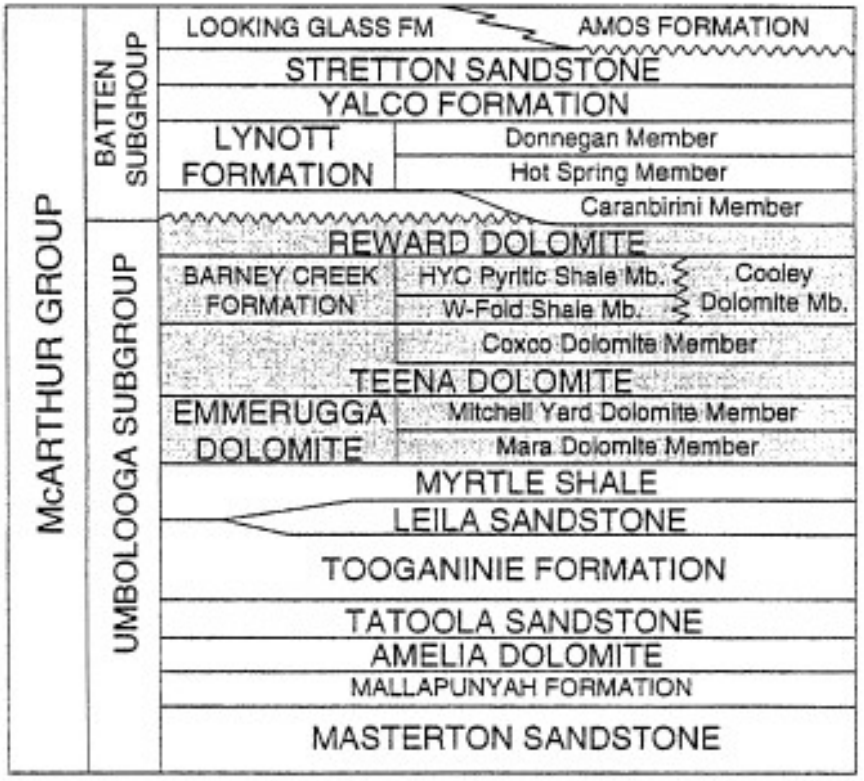

Stratigraphic column of the southern McArthur basin (modified after Pietsch et al., 1991).

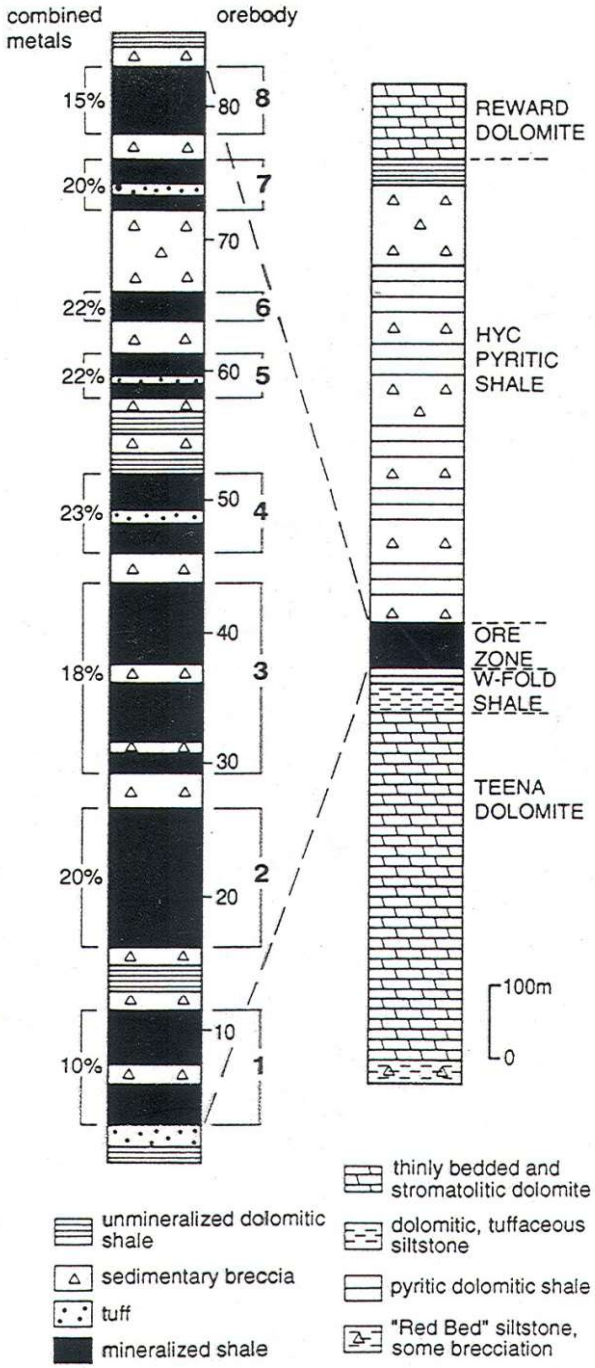

Simplified stratigraphic section for the mineralized zone at HYC (adapted from Eldridge et al., 1993), showing the relationship between sedimentary mass-flow breccias and the Pb-Zn mineralized shales that comprise the eight stratiform orebodies.

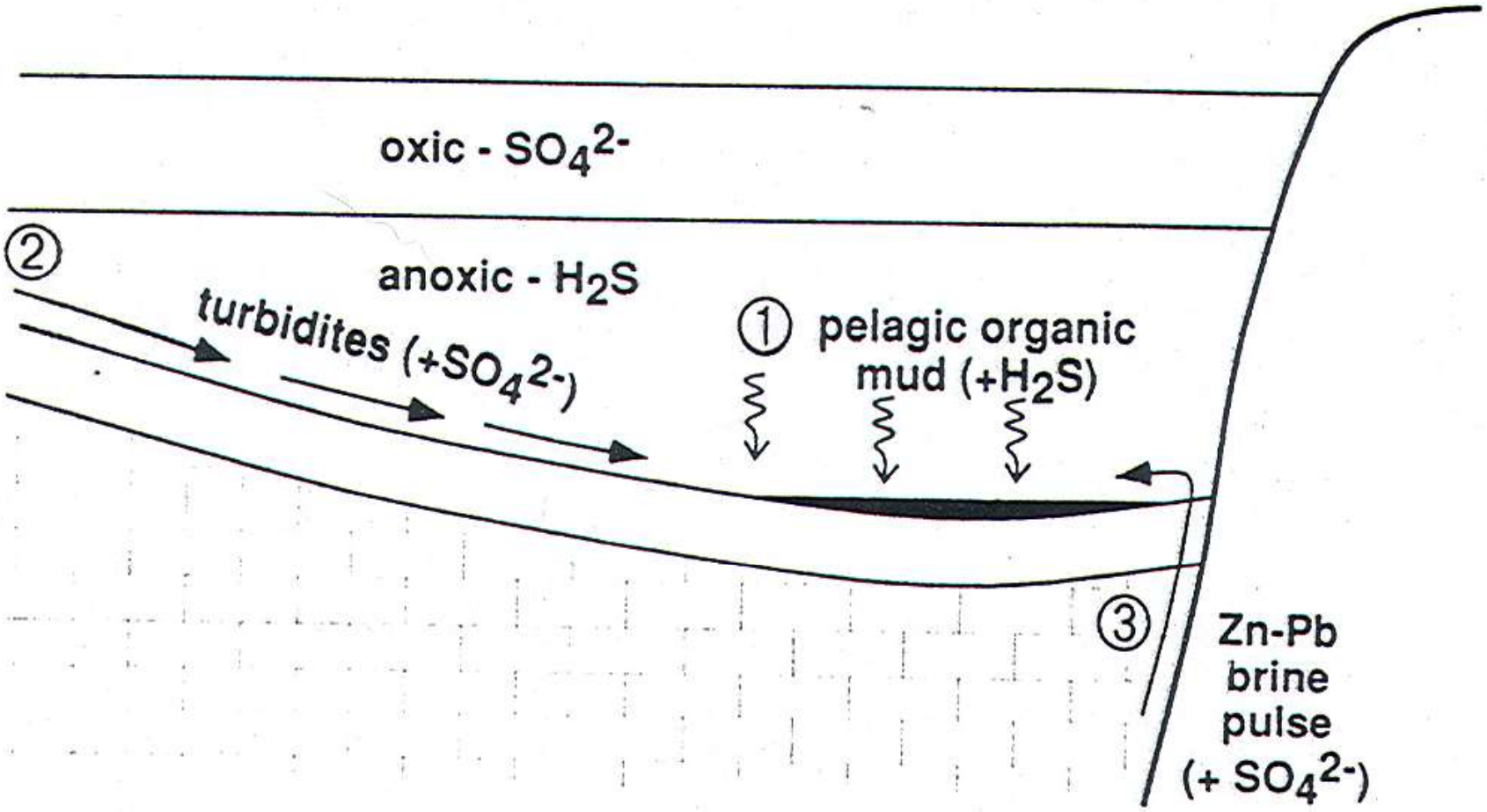

Diagrammatic representation of the three proposed components of deposition during ore formation at HYC. (1) Pelagic mud from anoxic water column; (2) oxic quartz-carbonate turbidity flows from the basin margins; (3) Zn-Pb-bearing brine pulses migrating along active proximal faults.

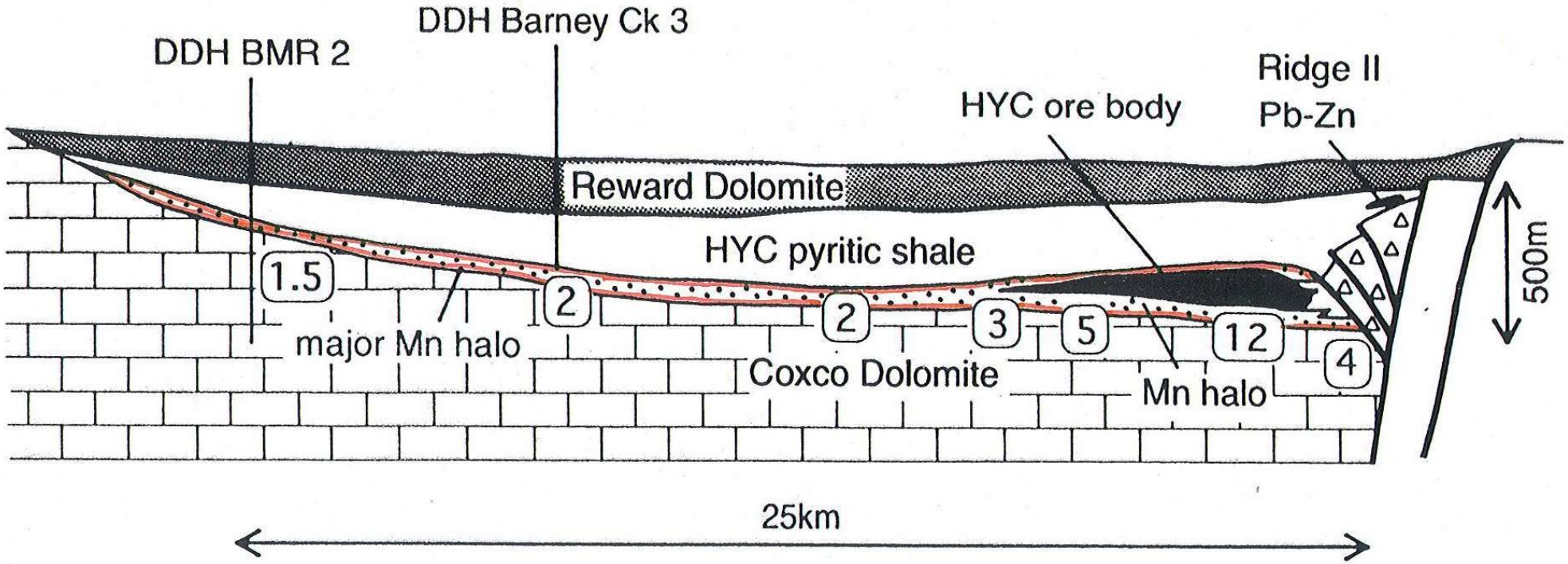

Reconstruction of the manganese halo related to the HYC deposit, interpreted from drill hole analyses in Corbett et al. (1975), plus additional data from this study. The numbers in the boxes are the maximum value of wt percent MnO in dolomite in the W-Fold Shale, determined from the whole-rock analyses, calculated using the procedure of Large and McGoldrick (in press).

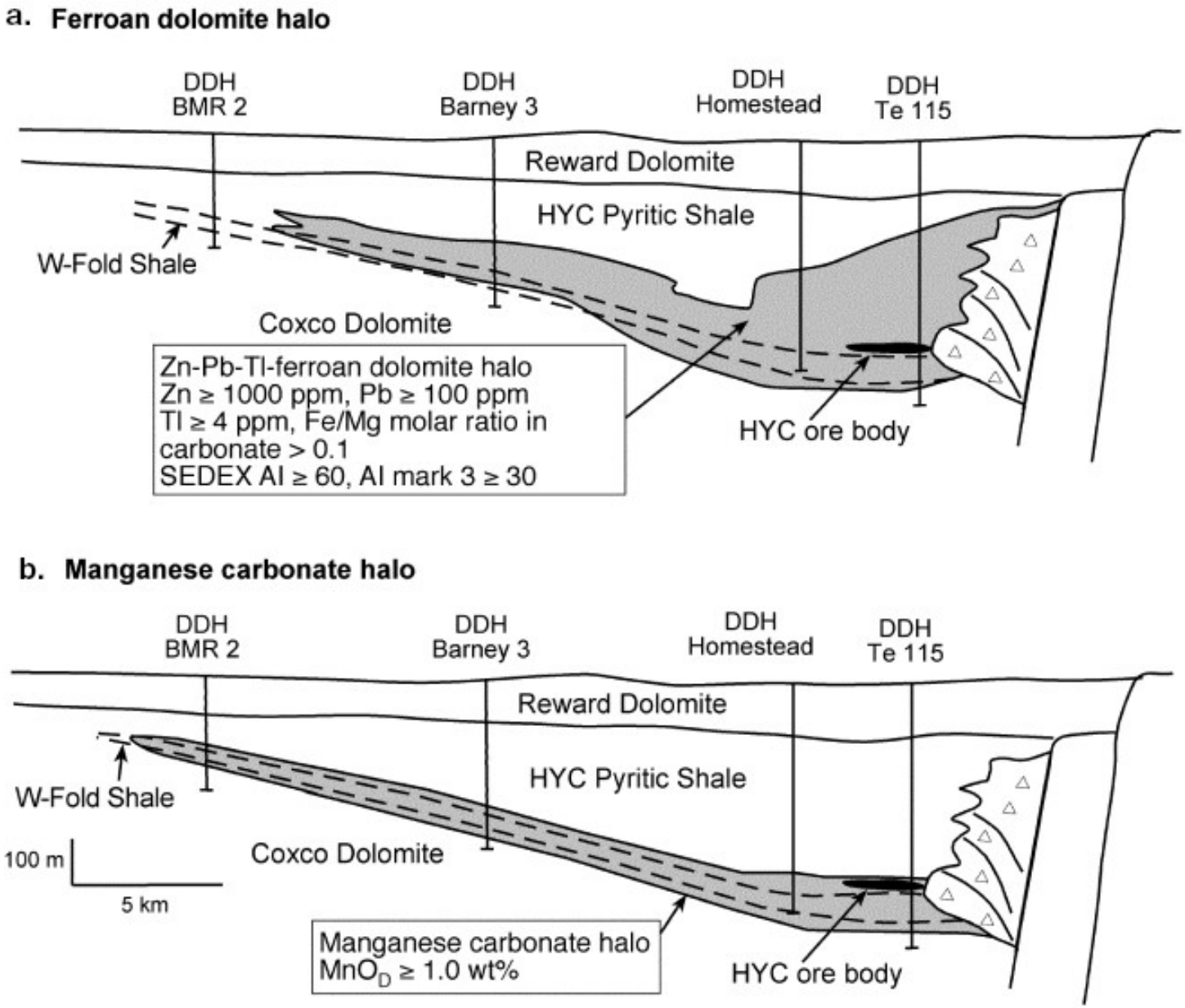

Lithogeochemical halo model for the HYC deposit from Large et al. (2000). AI mark 3 = 100(FeO + 10 MnO)/(FeO + 10 MnO + MgO + Al_2O_3), MnO_d = MnO × 30.41/CaO, SEDEX AI = 100(FeO + 10 MnO)/(FeO + 10 MnO + MgO).

a. Oxygen isotope halo

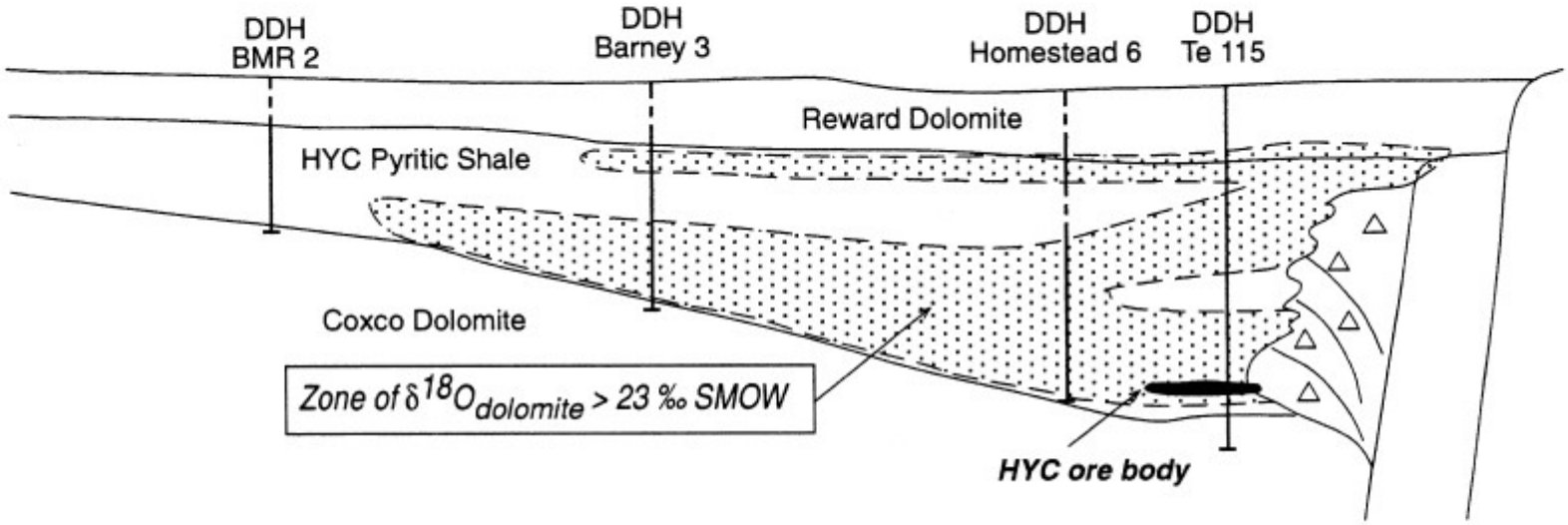

b. Carbon isotope halo

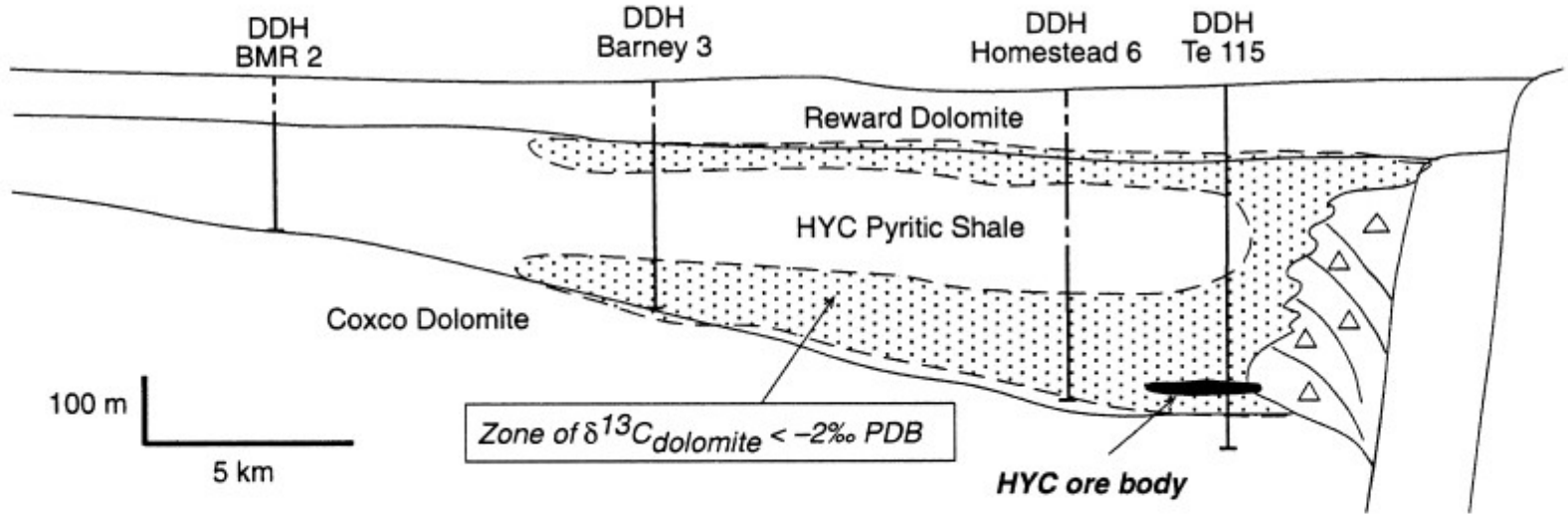

Schematic representation of the zones of enriched ^{18}O and depleted ^{13}C in dolomitic sediments of the Barney Creek Formation along a southwest-trending section line through HYC and the drill holes sampled in this study.

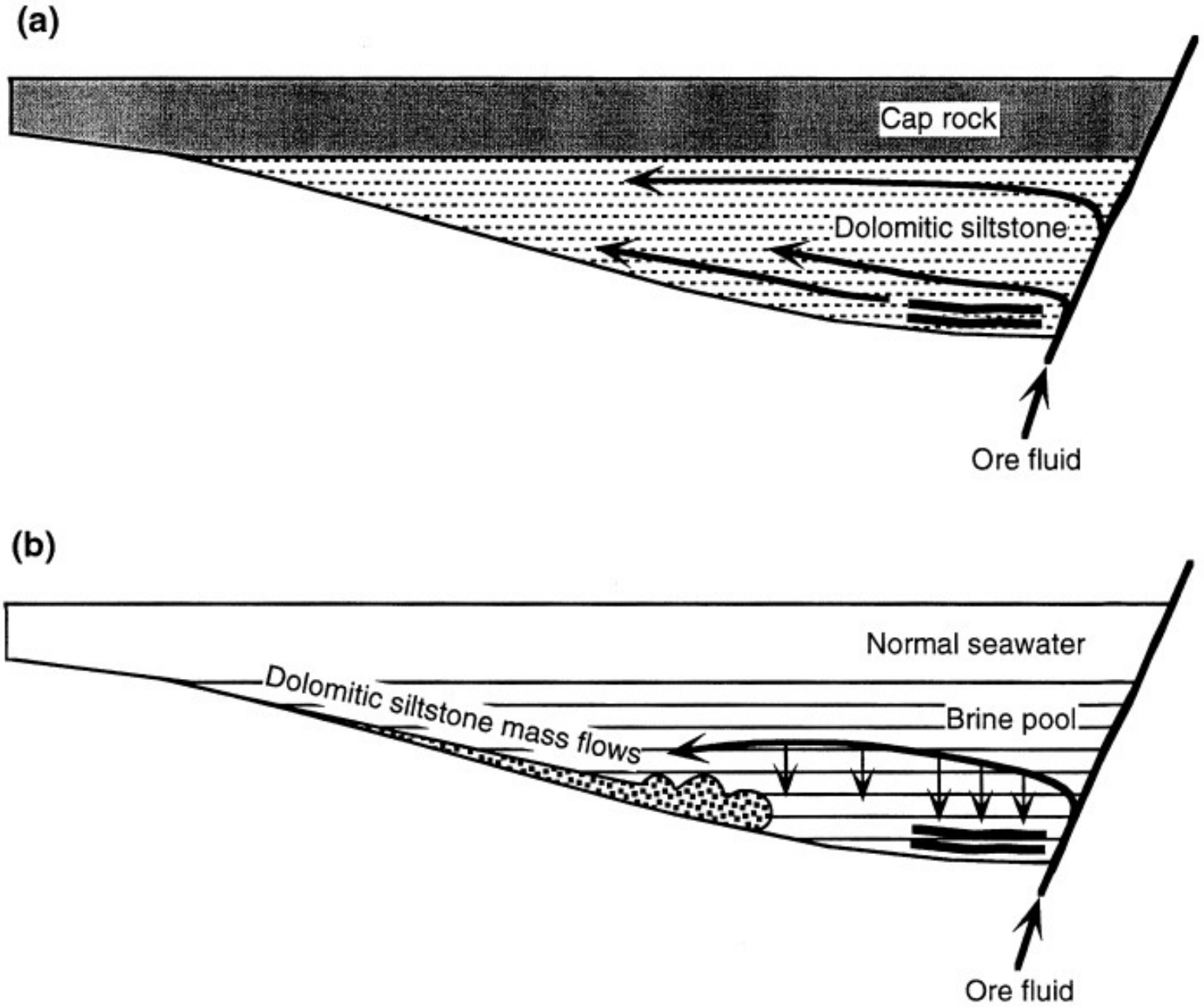

. Cross section depicting HYC lithogeochemical and isotope halo formation. a) Replacement below the basin floor. b) Exhalation on the basin floor.

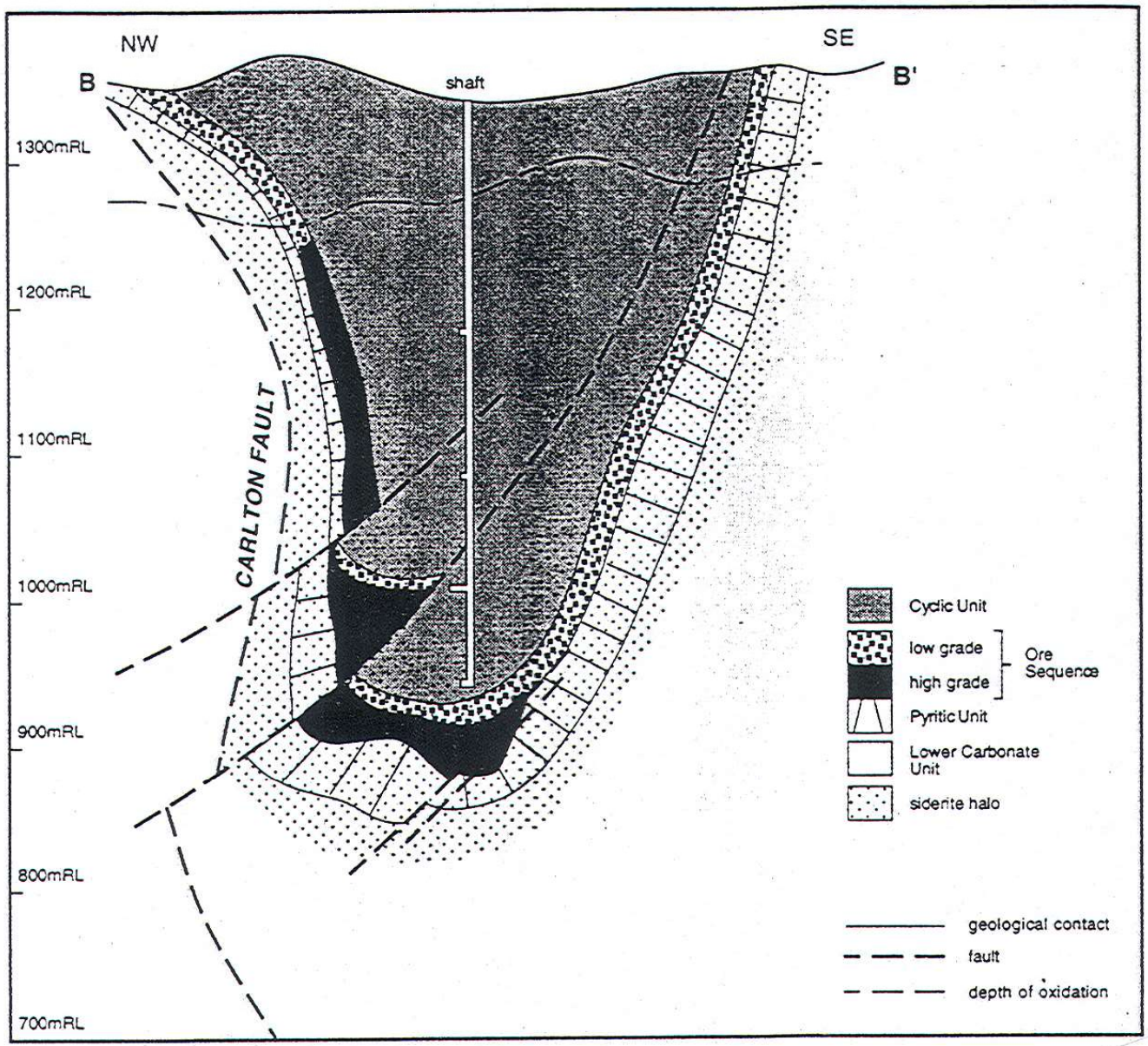

Typical geological cross section. Lady Loretta deposit (section 2300), modified from Hancock and Purvis (1990) and Carr (1984).

LADY LORETTA HALO MODEL

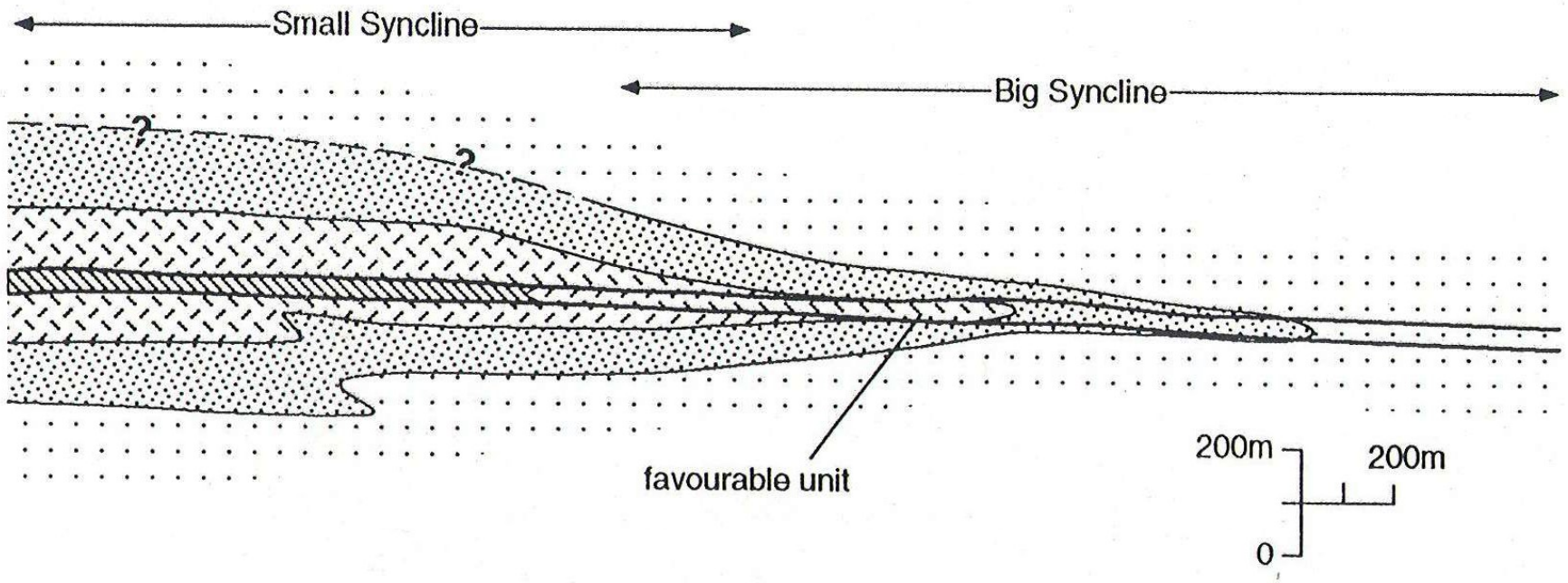

		Zn	Pb ppm	dominant Carbonate	Tl ppm	MnO %	CaO %	SEDEX AI	MnO_d/s %	Metal Index
Zn-Pb ore		>5%	>1000	siderite	>50	0.1-0.4	0-1	80-100	1-10	$>8x10^4$
Siderite halo		100ppm to 5%	10-1000	siderite	2-50	0.01-1	0-1	60-100	1-10	$2x10^3$-$3x10^4$
Ankerite halo		20-200ppm	<70	ankerite	2-50	0.01-0.04	1-2	38-60	0.4-0.7	$2-7x10^3$
Dolomite halo		<30ppm	<20	dolomite	<2	<0.01	5-10	10-40	<0.3	$<3x10^3$

Halo model (pre-folding) for the Lady Loretta deposit based on geochemical data from the Small Syncline and Big Syncline.

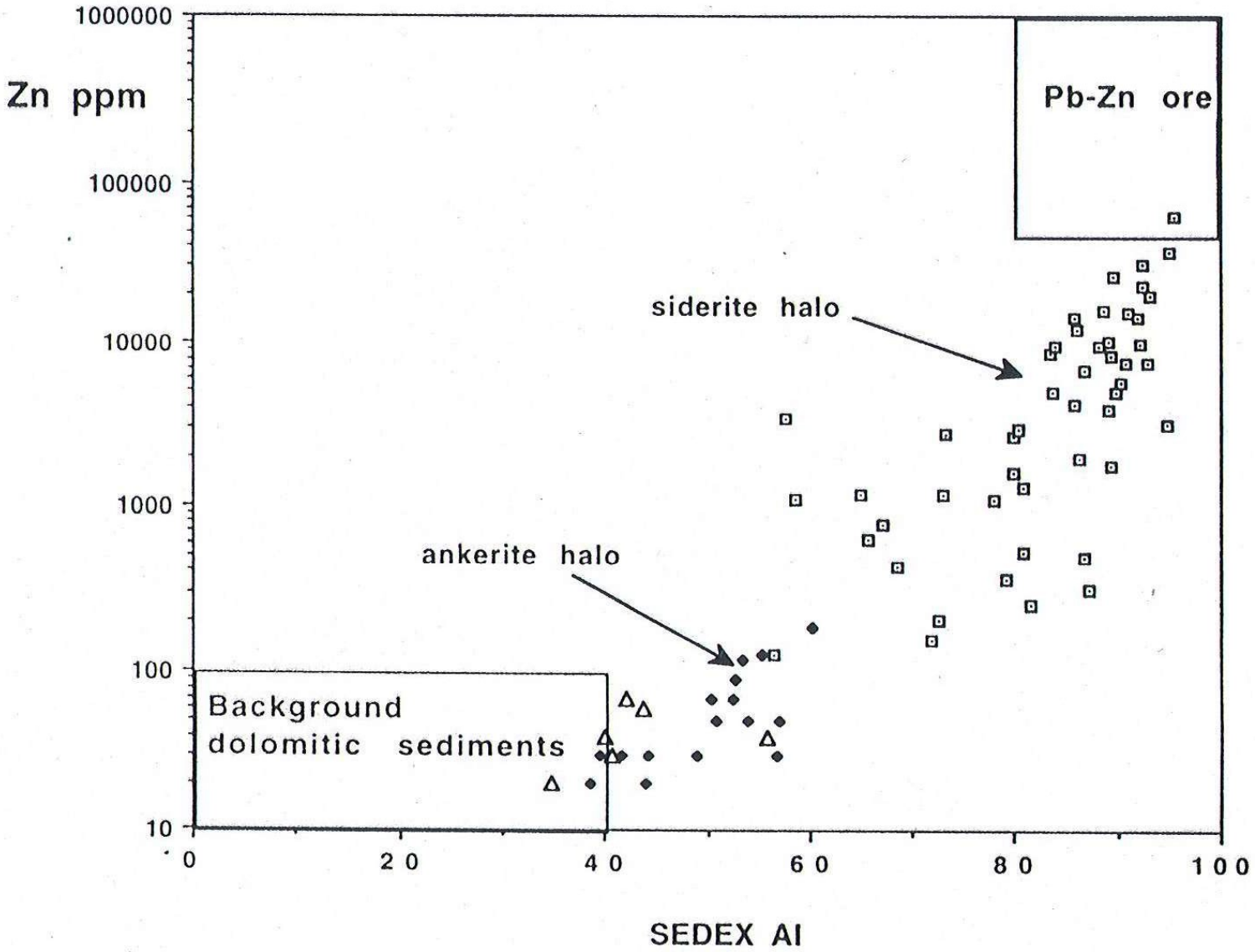

Positive trend of increasing SEDEX alteration index with zinc content for sediments in the Small Syncline at Lady Loretta. The field for background dolomitic sediments in the Lawn Hill Platform is based on unpublished data.

ΒΙΒΛΙΟΓΡΑΦΙΑ

- Franklin, J.M., Gibson, H.L., Jonasson, I,R., & Galley, A.G., (2005), Volcanogenic massive sulphide deposits: *Economic Geology, 100th Anniversary Issue*, pp. 523-560.
- Large, R.L., and McGoldrick, P.J. (1998) Lithogeochemical halos and geochemical vectors to stratiform sediment hosted Zn–Pb–Ag deposits, 1. Lady Loretta Deposit, Queensland, *Journal of Geochemical Exploration* **63**: 37-56
- Large R.R., Bull S.W., and Winefield, P.R. (2001) Carbon and Oxygen Isotope Halo in Carbonates Related to the McArthur River (HYC) Zn-Pb-Ag Deposit, North Australia: Implications for Sedimentation, Ore Genesis, and Mineral Exploration. *Econ. Geol.* **96**: 1567-1593.
- Leach D.L., Sangster D.F., Kelley K.D., Large R.R., Garven, G., Allen, C.R.., Gutzmer, J. and Walters, S., (2005) Sediment-hosted Pb–Zn deposits: a global perspective. *Economic Geology 100th Anniversary Issue*, pp. 561-607.
- Ohmoto, H. (1996) Formation of volcanogenic massive sulfide deposits: The Kuroko perspective. *Ore Geology Reviews* ***10***: 135-177.
- Petersen, S., Herzig, P.M., and Hannington, M.D. (2000) Third dimension of a presently forming VMS deposit: TAG hydrothermal mound, Mid-Atlantic Ridge, 26ºN. *Mineralium Deposita* **35**: 233-259.